NASA Reference Publication 1026

An Assessment of the Effect of Supersonic Aircraft Operations on the Stratospheric Ozone Content

I. G. Poppoff, R. C. Whitten, R. P. Turco,
and L. A. Capone

AUGUST 1978

NASA

NASA Reference Publication 1026

An Assessment of the Effect of Supersonic Aircraft Operations on the Stratospheric Ozone Content

I. G. Poppoff and R. C. Whitten
Ames Research Center
Moffett Field, California

R. P. Turco
R and D Associates
Marina del Rey, California

L. A. Capone
San Jose State University
San Jose, California

TABLE OF CONTENTS

AN ASSESSMENT OF THE EFFECT OF SUPERSONIC AIRCRAFT OPERATIONS

ON THE STRATOSPHERIC OZONE CONTENT

I. G. Poppoff, R. C. Whitten, R. P. Turco,* and L. A. Capone†

Ames Research Center

SUMMARY

The purpose of this assessment of the potential effects of advanced supersonic aircraft on stratospheric ozone is to guide NASA programs for the development of supersonic aircraft technology. Two types of advanced SST design concepts were studied. Type A is the AST-100 with a cruise altitude of 20 km and a speed of Mach 2.7. Type B is a concept using variable cycle engines; it has a cruise altitude of 17.5 km and a speed of Mach 2.3.

From the results of the present assessment it appears that realistic SST fleet sizes should not cause concern with regard to the depletion of the total ozone overburden. For example, the NO_x emission of 100 Type-A aircraft will cause the ozone overburden to *increase* by 0.03% to 0.12% depending on which vertical transport parameterization is used. For 100 Type-B aircraft, the increase is calculated to be 0.11% to 0.13%; the principal difference between the predictions for Type-A and Type-B aircraft is the nominal cruise altitude. These ozone changes can be compared with the prediction of a global average 0.88% ozone *decrease* (for 100 large SST's flying at 20 km) made in 1974 by the DOT's Climatic Impact Assessment Program. The differences between this assessment and the CIAP assessments are due primarily to important changes in values of chemical rate constants.

Interestingly, as engine technology advances (i.e., NO_x emitted by aircraft engines decreases) the importance of water vapor emissions increases. For example, if far-term engine technology is assumed for the 100 Type-A aircraft, it is predicted that the ozone overburden will be depleted by $0 - 0.06\%$, depending on the vertical transport parameterization assumed.

Aircraft assessments should be treated with caution. Knowledge of the stratosphere is still expanding, measurements and theories are not yet reconciled, and many key measurements have not yet been made because they are either too difficult or too expensive or both. The important methane chemistry in the lower stratosphere is not fully documented and it does not appear at present that water vapor effects are properly corrected for thermal feedback effects. It should also be noted that the change in SST assessments over the past year has been due largely to the recognition of potential ozone increases in the lower stratosphere that offset the potential decreases in the upper stratosphere. Hence, although the *total* ozone overburden appears to be affected only slightly according to assessment models, the *distribution* of ozone with altitude is affected more significantly. At this time, however, it is not possible to evaluate the meteorological consequences of such an ozone redistribution.

*Research Scientist, R and D Associates, Marina del Rey, California.

†Research Associate, San Jose State University, San Jose, California.

1. INTRODUCTION

This report presents an assessment of the potential effect of future aircraft operations on the abundance and distribution of ozone in the stratosphere. The reasons for concern about the possibility of modifying the stratospheric ozone content — by even a small fraction — are well known and are not discussed here; the interested reader is referred to the CIAP "Report of Findings" (ref. 1); the National Academy of Sciences reports, "Environmental Impact of Stratospheric Flight" (ref. 2); and "Halocarbons: Environmental Effects of Chlorofluoromethane Release" (ref. 3).

The assessment reported here was undertaken because of NASA's desire for an up-to-date evaluation to guide programs for the development of supersonic aircraft (SST) technology and improved engine designs. Since the publication of SST assessments by the DOT's Climatic Impact Assessment Program (CIAP) (ref. 4) and by the NAS Climatic Impact Committee, some important reaction rate constants and atmospheric constituent abundances have been measured or remeasured. In addition, stratospheric models have been refined with respect to the effects of diurnal variations and scattered light. In recent months the Lawrence Livermore Laboratory group has also updated, for the Department of Transportation, their evaluation of the environmental impact of "Concorde" type SST's on the upper atmosphere (ref. 5).

Shortly before this assessment was started, NASA sponsored a comprehensive workshop on stratospheric aeronomy and meteorology in order to arrive at an estimate of the effects that chlorofluoromethanes (CFM's) might have on the global amount of ozone. The NASA CFM Assessment Workshop, held at Warrenton, Virginia in January 1977, included a thorough review of photochemical reaction rate data and a detailed comparison of one-dimensional (1-D) stratospheric models. At a subsequent workshop, held in July 1977 at the Goddard Space Flight Center, the reaction rate data and model comparisons were updated again. Accordingly, for this aircraft assessment we utilize most of the chemical rate constants recommended by the CFM Workshop (see ref. 6). We have also employed two one-dimensional (1-D) models for our calculations. The first is the NASA Ames/R and D Associates model of stratospheric and mesospheric trace constituents; the basic structure of the model is described in reference 7 although some of the model parameters have been updated for this assessment. The second 1-D model, which is normally used in support of the Ames two-dimensional (2-D) model (ref. 8), simulates tropospheric as well as stratospheric and mesospheric gas distributions. It has been utilized here to assess the magnitude of tropospheric ozone changes caused by stratospheric aircraft operations and to investigate the role of lower boundary conditions in calculating stratospheric ozone changes due to SST's. The calculated ozone perturbations that are given in this report have been made with the first model because it was found that the troposphere need not be included in SST simulations as long as the model lower boundary conditions are carefully chosen. The rationale for this approach is discussed in the report.

Unfortunately, a thorough comparison of two-dimensional models has never been made. Therefore, several groups with operational 2-D models were invited to participate in an aircraft assessment modeling workshop at Ames Research Center. For a variety of reasons, only two groups were able to participate; these were the Aerospace group (ref. 9) and the Ames Research Center group (ref. 8). The results of the two-dimensional model calculations were not available for this report and will therefore be reported separately.

2

It must be stressed that new information about the stratosphere is being made available almost continually. Hence, it should be understood that this SST assessment is based on our current understanding of stratospheric processes and numerical modeling techniques.

A brief chronology of events that occurred during the preparation of this report will illustrate the changing situation. Initially, it appeared that an increasing stratospheric chlorine content (due to CFM accumulation in the atmosphere) might affect the catalytic efficiency of ozone destruction by the nitrogen oxides in aircraft exhaust because the formation of chlorine nitrate ($ClONO_2$) might serve as an additional sink for these nitrogen oxides. Shortly thereafter, a new measurement was reported for the rate constant of the reaction, $NO + HO_2 \rightarrow NO_2 + OH$ (ref. 10). The new rate constant is about 30 times larger than the old value. As a consequence, the aeronomy of the lower stratosphere has had to be extensively re-examined. It turns out, for example, that both HO_2 and NO concentrations are effectively reduced by this reaction, and OH concentrations are dramatically increased. Enhanced OH leads to a more complete conversion of NO_2 into nitric acid, which diminishes the ozone catalytic activity of the nitrogen oxides. In addition, the faster $NO + HO_2$ reaction greatly increases the efficiency of ozone production by methane oxidation or "smog" chemistry. (A complete discussion is given in the text.) Thus, in a number of ways this one reaction rate measurement caused the assessment of SST effects to change radically, so much so that several recently published model studies of high-altitude aircraft effects on the stratosphere which did not include the new value of the rate constant (refs. 9, 11—13) have already become obsolete in many respects.

For the SST assessment presented here, we have made calculations specifically to test for the sensitivity of predicted ozone changes to several model parameters. We have also compared our calculations with those made recently by scientists at the Lawrence Livermore Laboratory. These tests and comparisons have revealed that predicted ozone alterations by SST's may be quite sensitive to the details of methane oxidation chemistry, the chlorine abundance of stratospheric air, the rate of reaction of ozone with HO_2, the aeronomic efficiency of hydrogen radical recombination, and the emission of water vapor by aircraft engines. The new importance of some of the parameters is due in large part to the recent revision of the rate constant for the $NO + HO_2$ reaction and the resultant enhancement in predicted model OH abundances. We will discuss these and related aspects of the SST problem more thoroughly in the following sections.

Since, in the future, we expect the emergence of new information that may affect our model calculations, we feel that it is not possible to make a conclusive assessment of SST effects on ozone at this time. Moreover, the present and projected abundances of anthropogenic chlorine in the atmosphere, and the possible increase in the background level of the oxides of nitrogen due to accelerating fertilizer usage, are still unresolved issues against which assessments of future aircraft effects must be judged. Therefore, the best that can be done now is to make an up-to-date assessment of the environmental effects of high-flying aircraft and to point out the areas of scientific knowledge which will require resolution before a better assessment can be achieved. We have taken this approach in our investigation.

In the following sections, we discuss aircraft characteristics, particularly nitrogen oxide and water vapor emissions as well as flight altitudes (section 2), and the details of our photochemical model, including the aeronomy of the stratosphere (section 3). Next we present the results of our assessment together with discussions of the sensitivity of those results to variations of important model parameters and of important uncertainties that affect our predictions (section 4). Finally, we

summarize our results in a general discussion (section 5). The reader who is interested only in the predictions of ozone change due to high altitude aircraft operations can read section 4 for a full discussion or section 5 for an encapsulated one.

2. AIRCRAFT CHARACTERISTICS

Several advanced supersonic transport design concepts are being studied by NASA. For this assessment, we have used one that is documented in a report by Baber and Swanson (ref. 14) and is based on the AST-100 airframe and a single-spool turbojet with variable turbine geometry and no augmentation (see appendix A). The documented flight conditions include a speed of Mach 2.7 and a cruise profile centered at 20 km altitude. The initial fuel consumption rate for this particular case is 44,100 kg/hr and the average consumption rate over the cruise portion of the flight is 37,800 kg/hr. We have also used a set of conditions that are representative of design concepts using the Pratt & Whitney VSCE 502 B variable cycle study engine and more advanced airframes. For these conditions, the cruise speed is Mach 2.3, the cruise profile is centered at 17.5 km altitude, the initial fuel consumption rate is 41,050 kg/hr (see appendix A), and the average fuel consumption rate is estimated to be 35,200 kg/hr. The essential difference between the two design concepts (insofar as potential effect on stratospheric ozone is concerned) is the flight altitude. The advanced aircraft design characteristics adopted for this assessment are summarized in table 1. In table 1, and throughout the report, the design documented by Baber and Swanson (ref. 14) is called Type A or the baseline aircraft; the lower altitude concept using the VSCE 502 B engine is called Type B.

TABLE 1.– AIRCRAFT CHARACTERISTICS

Type[a]	Nominal speed, Mach no.	Nominal altitude, km	Nominal average fuel flow rate, kg/hr	NO_x emission index (probe values), g NO_2/kg fuel
A	2.7	20	37,800	15.6 near term[b] 2–6 far term[b]
B	2.3	17.5	35,200	18 near term[b] 3–7 far term[b]

[a] Type A: AST-100 described by Baber and Swanson (ref. 1);
   Type B: uses four VSCE-502B engines (appendix A).

[b] See appendix A for discussion of near term and far term.

Our 1-D model calculations of aircraft effects are presented in terms of the total global deposition rate of NO_x (expressed as an equivalent amount of NO_2 in kilograms per year) by SST's operating at specific flight altitudes. One can use the data in table 1 to estimate the overall stratospheric NO_x injection rate for any presumed fleet of type A or B aircraft. Later we will present data which can be used to convert an NO_x injection rate into a stratospheric ozone column perturbation. Conversely, for each type of aircraft considered, one can use our ozone perturbation results, and the information in table 1, to estimate the number of aircraft that would produce a given effect (ozone change) in the stratosphere.

To facilitate the interconversion between the global deposition rate of NO_x (as NO_2), R_{NO_2}, and the equivalent number and characteristics of each type of aircraft, one can use the proportionality:

$$R_{NO_2} \propto N_{ac} M_F E_{NO_2} T_f \tag{1}$$

where N_{ac} is the number of operational aircraft, M_F is the total engine fuel flow rate at cruise conditions, E_{NO_2} is the NO_2 emission index, and T_f is the average flight time per aircraft per day. Curves corresponding to equation (1) for Type A aircraft are given in figure 1, which shows the total annual deposition rate of NO_2 in the stratosphere as a function of the number of aircraft. For near-term aircraft (fig. 1) we have adopted an emission index of 15.6 g NO_2/kg fuel and an average flight time of 7 hr/day per plane. For most of our far-term pollution estimates, we have chosen an emission index of 6 g NO_2/kg fuel for Type A engines (design goal is 2–6 g NO_2/kg fuel), a mean fuel flow rate of 37,800 kg/hr of aircraft operation, and an average flight time of 7 hr/day for future SST's. Using equation (1), we can easily adjust the stratospheric NO_x deposition rate, R_{NO_2}, in figure 1 to other fleet sizes, engine fuel flow rates, NO_2 emission indices, or aircraft flight times.

There is, however, uncertainty in our knowledge of NO_x concentrations in aircraft engine exhaust (ref. 15). The uncertainty is due to the disagreement between measurements using spectroscopic and probe techniques. The cause and extent of these uncertainties are being studied currently. When the discrepancy between the measurements is finally resolved, SST NO_x emission indices may have to be revised accordingly.

Water vapor is also emitted by aircraft engines. The amount is determined stoichiometrically in well-burned fuel and is equivalent to an emission index of about 1.3 kg H_2O/kg fuel.

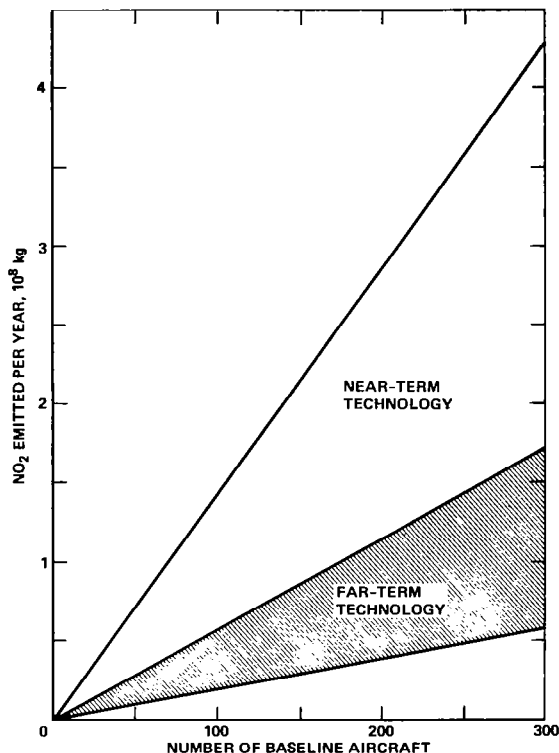Figure 1.— Total annual deposition rate of NO_2 in the stratosphere as a function of the number of aircraft.

3. THE PHOTOCHEMICAL MODEL

Two 1-D models have been utilized in this assessment. The basic model employed to make most of the assessment calculations is one used in the past to study the effects on the stratosphere and mesosphere of nitrogen oxides ($NO_x \equiv NO + NO_2$) ejected by SST engines or deposited by

5

rising nuclear fireballs, and of chlorine gases ($C\ell_X = HC\ell + C\ell O + C\ell + C\ell ONO_2 + HOC\ell$) emitted by space shuttle rocket motors or released during the photolysis of CFM's. A complete description of the basic model is given in reference 7, although we note that some of the results quoted therein are now outdated. For more details about the basic model and some of the predictions made with it, also see references 16–19. A second one-dimensional model has been used to confirm the predictions of the basic 1-D model. The second model has previously been used mainly in the development program for the Ames 2-D model; a description of the photochemical computational techniques is given by Whitten et al. (ref. 8). In this report calculated ozone effects due to SST's are given only for the first model because the results for the second model are very similar.

It is worth mentioning at this point that both of the 1-D models take into account scattered solar radiation above 300 nm, and utilize diurnally averaged photochemical rate constants for numerical predictions (ref. 20). All of the species concentrations presented in this report are equivalent to average daytime values (as opposed to 24-hr average values) unless otherwise specified.

Model Boundary Conditions

Our basic model has a lower boundary at 10 km. At this height it is an easy matter to set reasonable boundary conditions for most species (see ref. 7 for a thorough discussion of the model boundary conditions). For some of the important atmospheric constituents, no measurements are currently available for the upper troposphere and lower stratosphere and their boundary concentrations must therefore be estimated.

In our model, reactive radicals and atoms (e.g., O, OH, $C\ell$, CHO) are assigned a zero flux at 10 km; in this case, their concentrations near the lower boundary are controlled by photochemical reactions. For each long-lived species (e.g., O_3, CO_2, N_2O, CFM's) a concentration based on observational data is specified at 10 km; the model automatically establishes a flux at the boundary which acts to maintain this concentration (see ref. 7 for more details). The boundary flux involves a boundary "velocity," which is inversely related to the species residence time in the upper troposphere. We have assumed a boundary velocity of 1 cm/sec, which is a typical value; our results are not very sensitive to this parameter, however.

Compounds that can be removed by heterogeneous processes (rainout, washout) in the troposphere (e.g., H_2O_2, $HC\ell$, nitrogen oxides) are treated in the same way as the long-lived species, except that an estimated boundary concentration is used. For example, we assume a total mixing ratio of about 0.05 ppbv (parts per billion by volume) of NO_y ($\equiv N + NO + NO_2 + NO_3 + 2N_2O_5 + HNO_2 + HNO_3 + C\ell ONO_2$) at 10 km. We use this boundary concentration to compute the total boundary flux of NO_y just as we would for any individual model constituent, and then we determine the boundary flux of each nitrogen oxide component according to its instantaneous fraction of the total amount of NO_y.

Ambient water vapor is handled somewhat differently than the other species in our model; below 14 km, its concentrations are fixed at values corresponding to the U.S. Standard Atmosphere (ref. 21) water vapor profile; above 14 km, water vapor diffuses like the other gases, some of it being produced by methane oxidation.

The sources of active stratospheric chlorine ($C\ell_x$) in our model are the inert halocarbons $CF_2C\ell_2$, $CFC\ell_3$, $CC\ell_4$, and $CH_3C\ell$. The total mole fraction of chlorine atoms contained in these substances at 10 km is about 2.0 ppbv.

We have not included tropospheric ozone changes in our 1-D model assessment because of the extreme uncertainties in the ozone photochemistry of this region, including questions about the heterogeneous interactions occurring in the lower atmosphere, boundary-layer processes, and meteorological effects. However, since our second model has a troposphere, we have been able to check the implications of this modeling approximation. We have found, by comparing the predictions of the two models, that the ozone perturbations below 10 km due to SST's can be neglected. The fact that SST-induced changes in ozone and NO_x at 10 km are very small is amply documented in other recent work (e.g., see fig. 3.28 of ref. 15; and ref. 22). One reason for the negligible changes below 10 km due to NO_x injection by SST's is that, under most conditions, the SST source of NO_x represents only a small fraction of the total natural input of NO_x to the troposphere.

Stratospheric models that extend to the ground usually adjust the species concentrations in the upper troposphere by carefully balancing surface fluxes against "rainout" removal. At the present time, this procedure for including tropospheric processes in a model does not appear to be any more precise for an SST assessment than simply specifying the species concentrations in the upper troposphere, which is the approach that we have taken in our calculations.

Temperature Feedback Effects

The prediction of ozone perturbations with a 1-D model is, of course, severely limited by the necessity to treat radiation and transport as highly parameterized noninteractive one-dimensional processes. We have, in the past, made calculations using a model which included an empirical heating and cooling simulation; we found that for SST's the temperature changes caused by ozone depletions could alter chemical reaction rate coefficients in such a way that the depletions were decreased by only about 10% to 20%. However, for calculations where large ozone perturbations — and consequent atmospheric temperature changes — are involved, the simple energy balance models that are currently available are not capable of predicting the resulting coupled thermal-dynamical interactions.

All aircraft engines emit copious amounts of water vapor as a product of hydrocarbon combustion. Later in this report we will show that, because of its photochemical reactivity in air, water emitted by high-flying aircraft can result in net stratospheric ozone reductions. However, H_2O is an infrared-active molecule, and its release by SST's can affect the heat balance of the stratosphere. Some recent model calculations by Luther and Duewer (ref. 23) indicate that the thermal feedback effect of added water vapor can largely offset its chemical destruction of ozone. However, the Luther and Duewer calculations were not done for a realistic SST-induced change in the water vapor mixing ratio profile, but rather for an ambient water vapor profile scaled by a constant factor at each altitude. SST-injected water vapor actually accumulates near the height of injection; from this point the water vapor mixing ratio change decreases slowly toward higher altitudes and more rapidly toward lower altitudes. It has been pointed out by Luther et al. (ref. 24) and others that the coupling between atmospheric temperature structure and dynamics, which is neglected in 1-D thermal feedback calculations, could also have a significant impact on the results for water vapor ozone perturbations.

Because of the above-mentioned uncertainties associated with temperature feedback effects, we will give results for SST calculations both with and without water vapor injection, while omitting any thermal infrared radiation interactions. Hence, our model predictions can be used as an indication of the potential environmental effect of future SST fleet operations if the photochemical effect of water vapor emission is not mitigated by thermal radiation feedback.

Vertical Transport

One-dimensional models assume atmospheric transport by vertical "eddy" diffusion. Studies using 2-D models (refs. 9,11-13) have shown that horizontal transport influences the predicted latitudinal distribution of ozone perturbations due to NO_x from high-flying aircraft. Nonetheless, a preliminary comparison of one- and two-dimensional model calculations indicates that one-dimensional model predictions are useful for exploring the effects of photochemistry on the stratospheric ozone layer, since globally averaged 2-D model results are similar to 1-D model results.

Figure 2 shows three diffusion coefficient profiles which have been used in this assessment. One is a modified version of an ed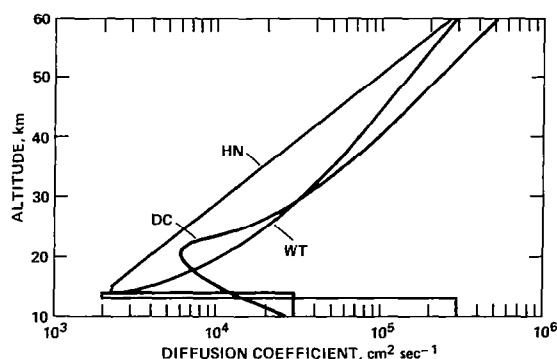dy diffusion profile first employed by Wofsy and McElroy (ref. 25) to match calculated atmospheric methane concentrations with observed values (WC in fig. 2). We have lowered the Wofsy-McElroy diffusion "tropopause" height from 16 km to 13 km (which we roughly estimate to be the surface-area-weighted, global-average tropopause altitude) and we have increased the diffusion coefficients above 20 km to obtain better agreement between predicted and measured methane concentrations in the upper stratosphere. The latter alteration has been required by changes in model photochemistry occurring since 1973. We will refer to the diffusion coefficient just described as a modified Wofsy-type (WT). A second diffusion coefficient (DC in fig. 2) has recently been proposed by Dickinson and Chang in the National Academy of Sciences report (ref. 3) on the effects of halocarbons on ozone, while the third is a coefficient originally suggested by Hunten (HN in fig. 2) (see refs. 15,26). Hereafter we will refer to these three diffusion coefficients as they are shown in figure 2, that is, as the WT, DC, and HN profiles, respectively.

Figure 2.— Atmospheric eddy profiles.

The location and magnitude of the minimum in an eddy diffusion profile are important parameters determining the simulated rate at which injected pollutants are removed from the lower stratosphere. The WT and HN diffusion profiles, with very effective transport barriers at the tropopause level, allow injected gases diffusing toward the troposphere to accumulate in the lower stratosphere. Johnston et al. (ref. 26) in their study of the excess atmospheric carbon 14 following several nuclear test explosions in the early 1960s, have demonstrated that a 1-D model using the HN diffusion profile closely reproduces the observed stratospheric residence time for this tracer. Johnston (private communication) has also found that a modified Wofsy-type diffusion profile with a tropopause at 13 km altitude is also quite compatible with the carbon 14 data. Our tracer calculations, some of which are presented in reference 7, agree with Johnston's work. It should be

noted, however, that the carbon 14 observational data may be too incomplete to serve as a reliable basis for selecting an eddy diffusion coefficient.

In a recent update by the High Altitude Pollution Program (HAPP) of post-CIAP studies, Oliver et al. (ref. 15) argue that the DC profile gives better results than the HN profile in a model calculation of the decay rates of radioactive zirconium 95 abundances observed after several Chinese nuclear bomb tests. Since these radioactive tracers are associated with aerosol particles, however, their residence times in the lower stratosphere are very sensitive to particle size (ref. 27) and may be affected by aerosol growth and coagulation processes. Bauer et al. (ref. 28) have refined the Zr^{95} analysis of Oliver et al. (ref. 15) and conclude that there is a substantial uncertainty in these calculations; even so, the average diffusion coefficient value deduced by Bauer et al. (ref. 28) for the altitude range between 11 and 20 km (about 7×10^3 cm^2/sec) is not in strong conflict with any of the diffusion profiles shown in figure 2.

By contrast with zirconium 95, carbon 14 is a gaseous tracer directly applicable to the determination of molecular residence times in the upper atmosphere. As it happens, a tracer model which uses the WT or HN diffusion profile gives fair agreement with the observed temporal decay of carbon 14 following its injection into the stratosphere, whereas a model which uses the DC diffusion profile gives poorer agreement. The stratospheric residence times of injected gases, such as NO_x or carbon 14 should be very similar; hence, it could be argued that the predictions of ozone reductions due to SST emissions using the WT or HN diffusion profiles might be more realistic than those using the DC profile.

Mason and Ostlund (ref. 29) have analyzed tritium oxide (HTO) distributions in the lower stratosphere, and have deduced a lifetime for water vapor below 18 km of about 2 yr, which is roughly consistent with other determinations. Moreover, they have detected large HTO concentration gradients in this region, gradients which could be associated with downward transport from a stratospheric source through a diffusion minimum at the tropopause.

Ambient Species Distributions and Vertical Transport

Observations of atmospheric trace gas constituents such as methane and nitrous oxide, together with a detailed model of air photochemistry, can be used to determine vertical eddy diffusion coefficients (refs. 25,30). In figures 3(a)-(c) our ambient 1-D model predictions are compared with some measurements of several long-lived species of this genre. Calculated (using the fast reaction rate for $NO + HO_2 \rightarrow NO_2 + OH$) and measured stratospheric mixing ratios for methane, nitrous oxide, and fluorocarbons 11 and 12 are shown.

Methane distributions are shown in figure 3(a). We see that the WT and DC diffusion coefficients give reasonable representations of some older methane observations in the upper stratosphere, while the HN profile more accurately reproduces a very recent methane measurement by Ackerman et al. (ref. 31). It must be noted, however, that calculated methane distributions in the stratosphere depend strongly on computed OH concentrations which are still very uncertain. Accordingly, agreement (or disagreement) between methane predictions and observations must be considered a rather weak confirmation (or disproof) of model validity.

9
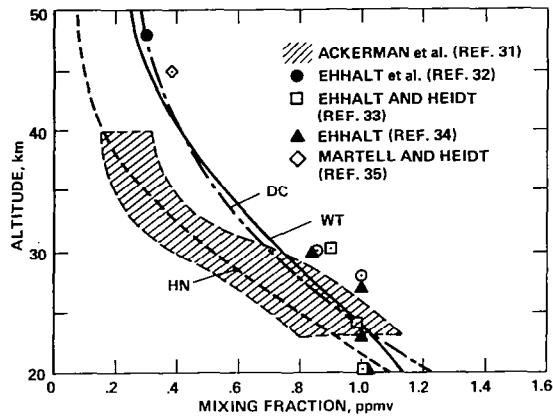
(a) Methane.
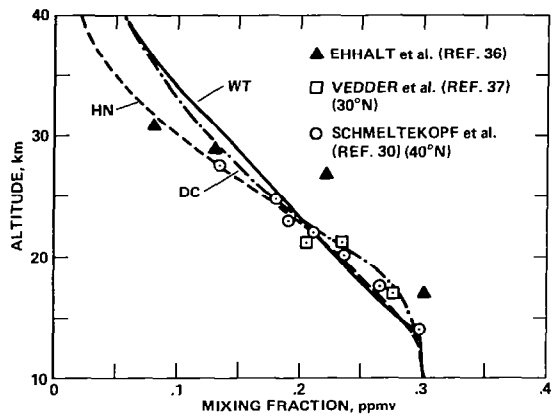
(b) Nitrous oxide.
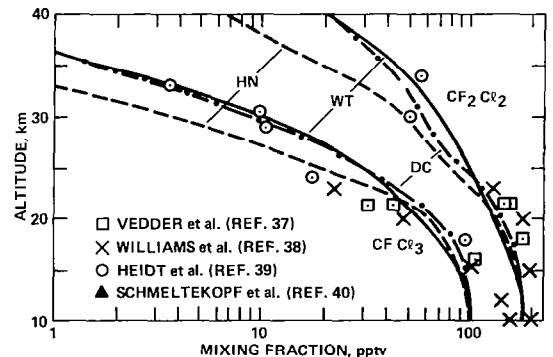
(c) Fluorocarbons 11 and 12.

Figure 3.— Calculated and measured stratospheric mixing ratio profiles.

For the N_2O and halocarbon distributions (figs. 3(b) and (c), respectively) the predictions for all of the diffusion coefficients are generally satisfactory. Many aeronomers currently believe that N_2O is a better determinant of stratospheric residence times than is methane. Schmeltekopf et al. (ref. 30) have recently used some of their new N_2O data to develop this concept. The average diffusion coefficient which fits all of their data collected over a wide range of latitudes, and altitudes from 17 to 27 km, coincides very closely with the WT profile shown in figure 2. When their low latitude (Panama) data are disregarded, the corresponding diffusion profile closely resembles the HN profile.

Ambient Species Distributions

Undisturbed ozone distributions calculated using the WT and DC eddy diffusion coefficients are shown in figure 4, and are compared to the empirical model of Krueger and Minzner (ref. 41). For clarity, the HN prediction is not shown. Although the WT and DC eddy diffusion coefficients give somewhat different results for the ozone profile, particularly below 30 km, several common features are apparent. For example, with the most up-to-date photochemistry, the total ozone columns above 10 km, about 3.7 and 3.4 mm STP for the WT and DC diffusivities, respectively, are near the high end of observed values. Above 40 km both the WT and DC ozone profiles lie substantially below the measured distribution shown in figure 4. In the case of the WT profile the predicted ozone concentrations near the peak are larger than many of the observations.

In figures 5—7, model calculations for the vertical daytime distribution of nitrogen, hydrogen, and chlorine oxides are contrasted with observed distributions. It should be noted that the predicted concentrations of several important stratospheric trace constituents (e.g., OH, CℓO) are not greatly affected by the selection of an eddy diffusion profile. However, as we have already pointed out, an important exception is found in the lowest part of the

10
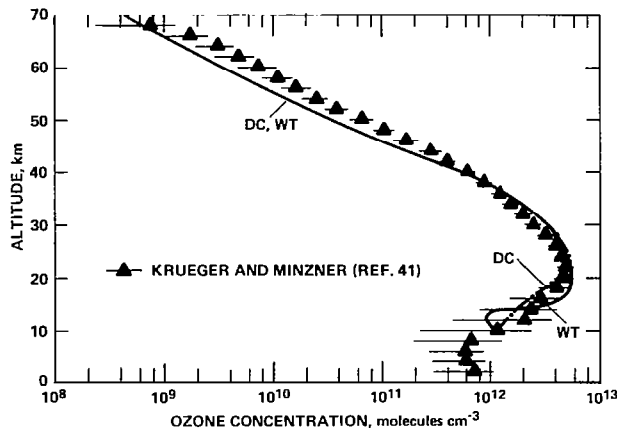
Figure 4.– Calculated and empirical model (ref. 41) ozone profiles; the one standard deviation variability of the model is shown by horizontal bars.
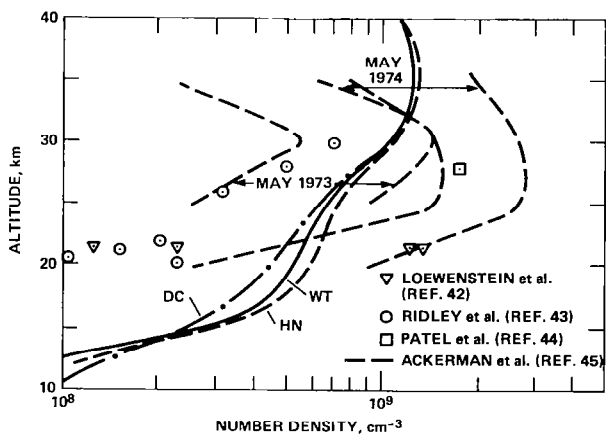
(a) Nitric oxide.
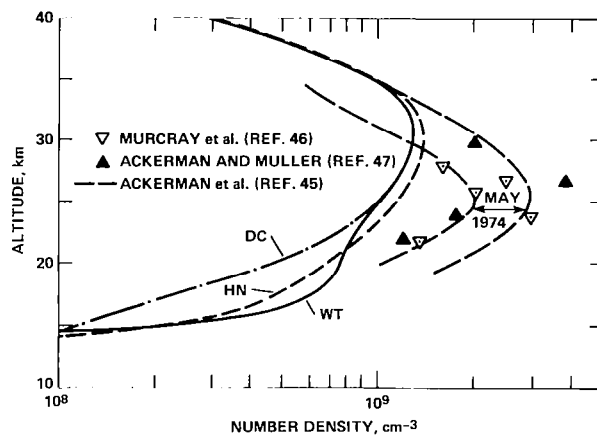
(b) Nitrogen dioxide.
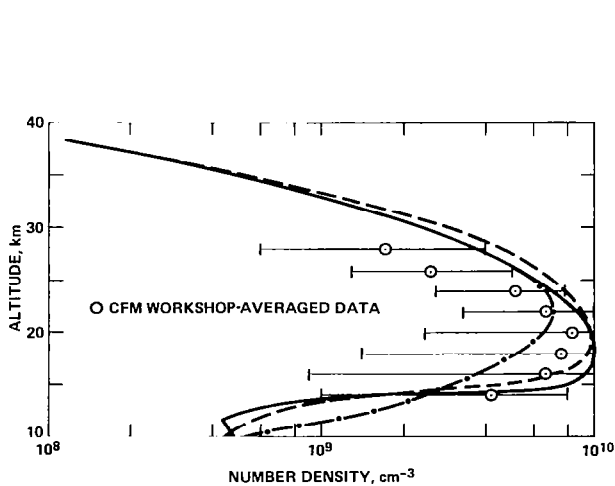
(c) Nitric acid.
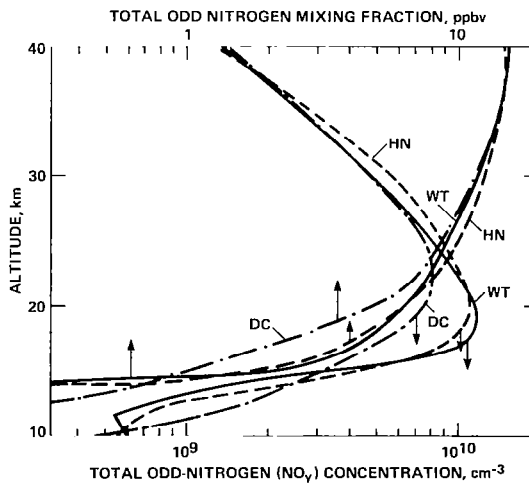
(d) Total odd-nitrogen $(N + NO + NO_2 + NO_3 + 2N_2O_5 + HNO_2 + HNO_3 + C\ell ONO_2)$.

Figure 5.– Calculated and observed vertical daytime distributions of the nitrogen oxides.

11
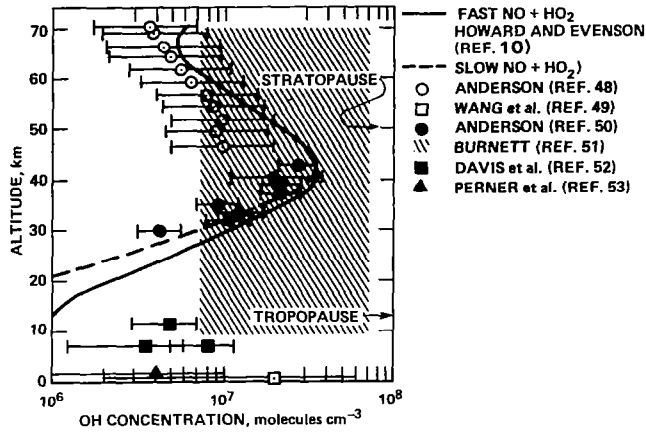
(a) Hydroxyl (OH).
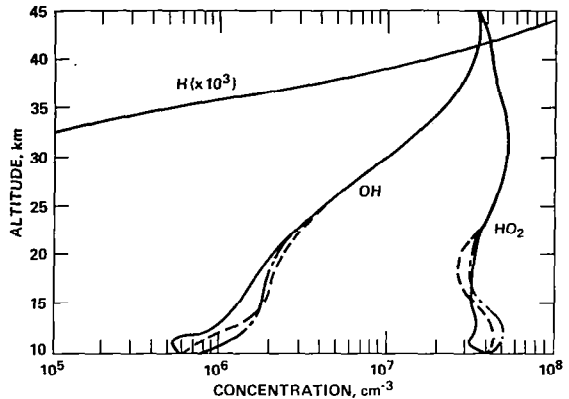
(b) HO$_x$ (H, OH, HO$_2$) theoretical profiles WT (———); DC (—·—); HN (------)

Figure 6.— Calculated and observed vertical daytime distributions of hydrogen radicals.
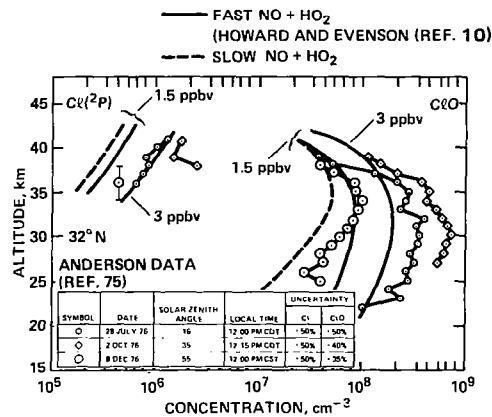
(a) Cℓ and CℓO. The data are from Anderson et al. (ref. 75).
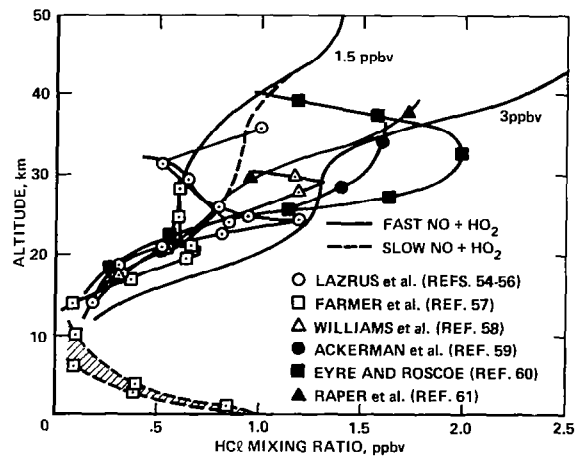
(b) HCℓ.
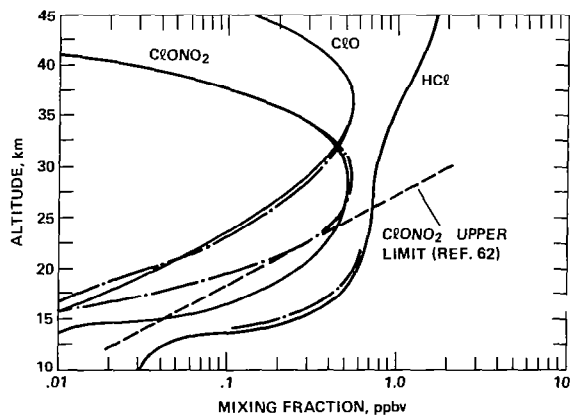
(c) CℓO, CℓONO$_2$, and HCℓ.

Figure 7.— Calculated and observed vertical daytime distributions of chlorine compounds. Eddy diffusivities: WT (———), DC (— ·—).

stratosphere (below 20 km) where the height of the diffusion minimum can greatly affect computed species abundances.

In figure 5 the WT, DC, and HN diffusion coefficients were used in the calculations with HNO_3 concentrations in figure 5(c) taken from Hudson (ref. 6).

Data sources for figure 6(a) — hydroxyl — are as follows: (1) Anderson (ref. 48), by monitoring scattered 306.4 nm sunlight over White Sands, New Mexico in April at a solar zenith angle of 86°; (2) Anderson (ref. 50), by observing laser-induced resonance fluorescence at about 309 nm over Palestine, Texas, in July and January at a zenith angle of 80°; (3) Wang et al. (ref. 49), by detection of laser-induced fluorescence centered at 309 nm at the ground near Dearborn, Michigan, during 4 days in August; (4) Burnett (ref. 51), by measuring the column-integrated resonance absorption of 308 nm sunlight from the ground at Fritz Peak Observatory in September and December (the integrated column has been uniformly distributed between 10 and 70 km); (5) Davis et al. (ref. 52), by observing laser-induced fluorescence at 309.5 nm at latitude 21° N and latitude 31° N in October in daylight; (6) Perner et al. (ref. 53), by measuring laser-light absorption at 307.95 nm in the air over Julich, Germany (lat. 51° N) in late summer and fall.

The measurement techniques for the data shown in figure 7(b) are as follows: (1) Lazrus et al. (refs. 54–56), using aircraft- and balloon-mounted filter paper collectors impregnated with a basic solution; (2) Farmer et al. (ref. 57), by infrared absorption spectroscopy at sunrise and sunset; (3) Williams et al. (ref. 58), by sunset infrared absorption spectroscopy; Eyre and Roscoe (ref. 60), using a balloon-borne pressure modulation radiometer; (4) Roper et al. (ref. 61), by infrared absorption spectroscopy at sunrise.

The results in figure 7(c) correspond to about 2 ppbv of total stratospheric chlorine. Concentration profiles are shown for the WT diffusion coefficient (solid line in fig. 7(c)) and for the DC coefficient (the − • − line in fig. 7(c)).

Using a one-dimensional model, it is presently impossible to match simultaneously all of the observational data for the stratospheric constituents; to obtain better overall computational agreement with the measurements shown in figures 3–7, and with other data not shown, large excursions from the NASA recommended rate constant values would probably be necessary, and a substantial revision of the eddy diffusion coefficient would be needed.

It is not clear at this time which type of eddy diffusivity profile is the better one to use for an SST assessment; each type appears to have some faults and virtues that cannot be checked definitively. On the other hand SST assessments, because of their strong dependence on processes occurring in the lower stratosphere, will be affected by the choice of an eddy diffusivity. The HN type, while very similar in shape to the WT type, yields different predictions of ozone change due to SST's. We have made most of our assessments with the WT and DC profiles because they are representative of substantially different *shapes* of the diffusion coefficient profile in the lower stratosphere and hence represent quite different lower stratospheric transport characteristics. These two diffusivity types provide a range of results which illustrate the importance of vertical transport in SST assessments, and indicate the sensitivity of these assessments to the transport parameterization.

13

Photochemical Rate Data

The chemical reaction and photodissociation rate coefficients used in our one-dimensional model calculations are essentially those recommended in the report of the NASA Chlorofluoro-methane (CFM) Assessment Workshop held in Warrenton, Virginia in January 1977 (ref. 6) and updated at the supplemental Workshop held at Goddard Space Flight Center on July 18—19, 1977. The model photochemical processes and rate constants are summarized in tables 2—6. The reactions of bromine and sulfur compounds, which are also included in our model, are not tabulated because they have little bearing on this work.

The new rate coefficient for the reaction between NO and HO_2

$$NO + HO_2 \rightarrow NO_2 + OH \tag{2}$$

has been measured by Howard and Evenson (refs. 10,66) at room temperature. The measurement is discussed at length in the CFM Workshop report (ref. 6). Later, we will discuss the implications of reaction (2) for SST assessments.

A reaction similar to reaction (2) occurs between NO and CH_3O_2. The CFM Workshop panel had assumed that the rate constant for this process is small, by analogy with the older rate constant of reaction (2). However, Cox (ref. 64) has determined a lower limit for the rate coefficient of about 1.5×10^{-12} cm^3 sec^{-1}. In accordance with this result, and in light of the newer measurement for reaction (2), we have selected a rate constant of 2.0×10^{-12} cm^3 sec^{-1} for the $NO + CH_3O_2$ reaction (see table 4).

In our model, photodissociation rates are computed using the Workshop recommended solar fluxes and absorption cross sections where possible and the computational technique described in reference 7 (also, see ref. 65).

The CFM Workshop panel originally recommended the H_2O_2 absorption cross sections tabulated by CIAP (ref. 4, vol. 1, pp. 5—186; 5—254); unfortunately, H_2O_2 absorption cross section data at wavelengths greater than 255 nm were not included in that tabulation. In earlier studies of H_2O_2 photolysis (e.g., see refs. 65,67,68) the long wavelength absorption "wing" observed by Urey et al. (ref. 69) had been used to extend the H_2O_2 absorption spectrum up to 310 nm; recent measurements have confirmed the existence of this weak long-wavelength H_2O_2 absorption (ref. 70; DeMore, private communication). If one neglects the long wavelength absorption "wing" of H_2O_2, significantly lower H_2O_2 photolysis rates are computed for the lower stratosphere; in this case the H_2O_2 abundance is limited primarily by reaction with OH and diffusion. In figure 8, for example, we show computed H_2O_2 photodissociation rates and concentrations with and without the long wavelength absorption. Obviously, even a small amount of H_2O_2 absorption above the ozone Hartley band cutoff (~300 nm) can control H_2O_2 concentrations below 30 km. Therefore, in order to achieve a more realistic assessment, we have included H_2O_2 absorption above 255 nm in our calculations, using the cross sections of Molina et al. (ref. 70) rather than those from the CIAP report. (Although the data of Molina et al. extend out to 350 nm, the cross sections (σ) are shown only out to 320 nm.) (We have investigated the effect on the CFM assessments of ignoring H_2O_2 photolysis above 255 nm. The predicted ozone depletions are reduced by about 10% to 20%. This is because slow H_2O_2 photolysis leads to slightly decreased OH abundances in the stratosphere, and therefore slightly less chlorine activity with respect to ozone.)

14

TABLE 2.– REACTION RATE CONSTANTS FOR THE O-N-H SYSTEM

Reaction	Rate constant[a]	Note	Reaction	Rate constant[a]	Note
$O + O_2 + M \rightarrow O_3 + M$	$1.1 \times 10^{-34} e^{520/T}$	b	$N + O_3 \rightarrow NO + O_2$	$2.0 \times 10^{-11} e^{-1070/T}$	
$O + O + M \rightarrow O_2 + M$	$3.0 \times 10^{-33} (300/T)^3$	b	$N + NO \rightarrow O + N_2$	$8.2 \times 10^{-11} e^{-410/T}$	
$O + O_3 \rightarrow O_2 + O_2(^1\Sigma_g^+)$	$1.9 \times 10^{-11} e^{-2300/T}$	b	$N + O_2 \rightarrow NO + O$	$5.5 \times 10^{-12} e^{-3220/T}$	
$O + OH \rightarrow H + O_2$	4.2×10^{-11}		$N + NO_2 \rightarrow N_2O + O$	$2.0 \times 10^{-11} e^{-800/T}$	
$O_3 + H \rightarrow OH + O_2$	$1.2 \times 10^{-10} e^{-560/T}$				
			$NO_2 + O_3 \rightarrow NO_3 + O_2$	$1.2 \times 10^{-13} e^{-2450/T}$	
$O + HO_2 \rightarrow OH + O_2$	3.5×10^{-11}		$NO_2 + O + M \rightarrow NO_3 + M$		b, c
$O_3 + OH \rightarrow HO_2 + O_2$	$1.5 \times 10^{-12} e^{-1000/T}$		$NO + NO_3 \rightarrow NO_2 + NO_2$	8.7×10^{-12}	b
$H + O_2 + M \rightarrow HO_2 + M$	$2.1 \times 10^{-32} e^{290/T}$		$NO_2 + NO_3 + M \rightarrow N_2O_5 + M$		b, c
$NO + O_3 \rightarrow NO_2 + O_2$	$2.1 \times 10^{-12} e^{-1450/T}$		$N_2O_5 + M \rightarrow NO_2 + NO_3 + M$		b, c
$O + NO_2 \rightarrow NO + O_2$	9.1×10^{-12}				
			$NO + HO_2 \rightarrow NO_2 + OH$	8.0×10^{-12}	
$NO + O + M \rightarrow NO_2 + M$	$1.6 \times 10^{-32} e^{584/T}$		$NO_2 + H \rightarrow NO + OH$	$5.8 \times 10^{-10} e^{-740/T}$	b
$OH + OH \rightarrow H_2O + O$	$1.0 \times 10^{-11} e^{550/T}$		$NO_2 + OH + M \rightarrow HNO_3 + M$		d
$OH + HO_2 \rightarrow H_2O + O_2$	3.0×10^{-11}		$HNO_3 + O \rightarrow OH + NO_3$	1.0×10^{-14}	b
$H + HO_2 \rightarrow OH + OH$	$2.8 \times 10^{-10} e^{-1000/T}$	b	$HNO_3 + OH \rightarrow H_2O + NO_3$	8.0×10^{-14}	
$H + HO_2 \rightarrow H_2 + O_2$	$3.2 \times 10^{-11} e^{-500/T}$	b			
			$NO + OH + M \rightarrow HNO_2 + M$	$1.8 \times 10^{-32} e^{1135/T}$	b
$H + HO_2 \rightarrow H_2O + O$	$1.6 \times 10^{-11} e^{-500/T}$	b	$HNO_2 + O \rightarrow OH + NO_2$	1.0×10^{-14}	b
$HO_2 + HO_2 \rightarrow H_2O_2 + O_2$	2.5×10^{-12}		$HNO_2 + OH \rightarrow H_2O + NO_2$	8.0×10^{-14}	
$H_2O_2 + OH \rightarrow H_2O + HO_2$	$1.0 \times 10^{-11} e^{-750/T}$		$O + H_2 \rightarrow OH + H$	$3.0 \times 10^{-14} T e^{-4480/T}$	b
$H_2O_2 + O \rightarrow OH + HO_2$	$2.8 \times 10^{-12} e^{-2125/T}$		$OH + H_2 \rightarrow H_2O + H$	$8.0 \times 10^{-12} e^{-2100/T}$	
$O_3 + HO_2 \rightarrow OH + O_2 + O_2$	$7.3 \times 10^{-14} e^{-1275/T}$				
			$OH + H \rightarrow O + H_2$	$1.4 \times 10^{-14} T e^{-3500/T}$	b
$OH + OH + M \rightarrow H_2O_2 + M$	$1.3 \times 10^{-32} e^{900/T}$				

[a] Rate constants are in molecule-cm-sec units. Unless otherwise noted, the rate constants are taken from Hudson (ref. 6).

[b] For detailed data references see the reaction tabulation in Turco and Whitten (ref. 19).

[c] For the complete pressure-dependent rate expression, see Turco and Whitten (ref. 19).

[d] The expression adopted for this rate constant is given in Hudson (ref. 6).

TABLE 3.– REACTION RATE CONSTANTS FOR EXCITED OXYGEN SPECIES

Reaction	Rate constant[a]	Note
$O(^1D) + N_2 \rightarrow O + N_2$	$2.0 \times 10^{-11} \, e^{107/T}$	
$O(^1D) + O_2 \rightarrow O + O_2(^1\Sigma_g^+)$	$2.9 \times 10^{-11} \, e^{67/T}$	
$O(^1D) + O_3 \rightarrow O_2 + O_2$	1.2×10^{-10}	
$O(^1D) + H_2O \rightarrow OH + OH$	2.3×10^{-10}	
$O(^1D) + N_2O \rightarrow NO + NO$	5.5×10^{-11}	
$O(^1D) + N_2O \rightarrow N_2 + O_2$	5.5×10^{-11}	
$O(^1D) + H_2 \rightarrow OH + H$	9.9×10^{-11}	
$O(^1D) + H_2O_2 \rightarrow H_2O + O_2$	3.0×10^{-10}	
$O(^1D) + N_2 + M \rightarrow N_2O + M$	3.5×10^{-37}	
$O_2(^1\Delta_g) + O_3 \rightarrow O + O_2 + O_2$	$4.5 \times 10^{-11} \, e^{-2800/T}$	b
$O_2(^1\Delta_g) + O_2 \rightarrow O_2 + O_2$	$2.2 \times 10^{-18} \left(\dfrac{T}{300}\right)^{0.8}$	b, c
$O_2(^1\Delta_g) \rightarrow O_2 + h\nu$	2.6×10^{-4}	b
$O_2(^1\Sigma_g^+) + O_3 \rightarrow O + O_2 + O_2$	2.3×10^{-11}	b
$O_2(^1\Sigma_g^+) + M \rightarrow O_2 + M$	1.8×10^{-15}	b
$O_2(^1\Sigma_g^+) \rightarrow O_2 + h\nu$	8.3×10^{-2}	b

[a]Rate constants are in molecule-cm-sec units. Unless otherwise noted, the rate constants are taken from Hudson (ref. 6).

[b]See Vlasov (ref. 63) for a recent discussion of excited state chemistry.

[c]For the complete pressure-dependent rate expression, see Turco and Whitten (ref. 19).

TABLE 4.– REACTION RATE CONSTANTS FOR CARBON COMPOUNDS

Reaction	Rate constant[a]	Note
$CO + O + M \rightarrow CO_2 + M$	$2.0 \times 10^{-33} \, e^{-2060/T}$	b
$CO + OH \rightarrow CO_2 + H$	1.4×10^{-13}	
$CH_4 + OH \rightarrow CH_3 + H_2O$	$2.4 \times 10^{-12} \, e^{-1720/T}$	
$CH_4 + O \rightarrow CH_3 + OH$	$2.8 \times 10^{-11} \, e^{-4350/T}$	b
$CH_4 + O(^1D) \rightarrow CH_3 + OH$	1.3×10^{-10}	
$CH_4 + O(^1D) \rightarrow CH_2O + H_2$	1.4×10^{-11}	
$CH_3 + O_2 + M \rightarrow CH_3O_2 + M$		b
$CH_3 + O \rightarrow CH_2O + H$	1.2×10^{-10}	b
$CH_2O + O \rightarrow CHO + OH$	$2.0 \times 10^{-11} \, e^{-1450/T}$	
$CH_2O + OH \rightarrow CHO + H_2O$	$3.0 \times 10^{-11} \, e^{-250/T}$	
$CHO + O_2 \rightarrow CO + HO_2$	6.0×10^{-12}	
$CHO + O \rightarrow CO + OH$	1.0×10^{-10}	b
$CHO + O \rightarrow CO_2 + H$	7.3×10^{-11}	b
$CH_3O_2 + NO \rightarrow CH_3O + NO_2$	2.0×10^{-12}	c
$CH_3O_2 + CH_3O_2 \rightarrow 2CH_3O + O_2$	2.0×10^{-15}	b
$CH_3O + O_2 \rightarrow CH_2O + HO_2$	$1.6 \times 10^{-13} \, e^{-3300/T}$	
$CH_3O_2 + HO_2 \rightarrow CH_4O_2 + O_2$	2.5×10^{-12}	b
$CH_4O_2 + OH \rightarrow CH_3O_2 + H_2O$	$1.0 \times 10^{-11} \, e^{-750/T}$	b
$CH_2 + O_2 \rightarrow CO_2 + H_2$	1.0×10^{-13}	b
$CH_2 + O_2 \rightarrow CHO + OH$	1.0×10^{-13}	b

[a]Rate constants are in molecule-cm-sec units. Unless otherwise noted, the rate constants are taken from Hudson (ref. 6).

[b]For detailed data references, see the reaction tabulation in Turco and Whitten (ref. 19).

[c]Based on a lower limit measurement of Cox (ref. 64).

TABLE 5.— PHOTODISSOCIATION RATES FOR O-N-H-C CONSTITUENTS

Photodissociation process[a]	Dissociation rate,[b] sec^{-1}
$O_2 + h\nu \xrightarrow{\lambda < 176\ nm} O(^1D) + O$	6.6×10^{-7}
$O_2 + h\nu \xrightarrow{176 \leqslant \lambda < 242\ nm} O + O$	5.9×10^{-8}
$O_3 + h\nu \xrightarrow{\lambda < 267\ nm} O_2(^1\Sigma_g^+) + O(^1D)$	2.1×10^{-4}
$O_3 + h\nu \xrightarrow{\lambda < 310\ nm} O_2(^1\Delta_g) + O(^1D)$	3.9×10^{-3}
$O_3 + h\nu \xrightarrow{310 < \lambda < 350\ nm} O_2(^1\Delta_g) + O$	8.1×10^{-4}
$O_3 + h\nu \xrightarrow{450 < \lambda < 750\ nm} O_2 + O$	2.3×10^{-4}
$NO + h\nu \to N + O$	6.1×10^{-6}
$NO_2 + h\nu \to NO + O$	6.4×10^{-3}
$NO_3 + h\nu \to NO + O_2$	2.0×10^{-2}
$\to NO_2 + O$	5.0×10^{-2}
$N_2O + h\nu \to N_2 + O(^1D)$	9.8×10^{-7}
$N_2O_5 + h\nu \to NO_2 + NO_2 + O$	3.1×10^{-4}
$HNO_2 + h\nu \to OH + NO$	4.8×10^{-4}
$HNO_3 + h\nu \to OH + NO_2$	9.0×10^{-5}
$H_2O + h\nu \to OH + H$	4.4×10^{-6}
$H_2O_2 + h\nu \to OH + OH$	7.1×10^{-5}
$HO_2 + h\nu \to OH + O$	4.4×10^{-4}
$CH_4 + h\nu \to CH_3 + H$	6.5×10^{-7}
$CH_4 + h\nu \to CH_2 + H_2$	1.9×10^{-6}
$CO_2 + h\nu \xrightarrow{\lambda < 167\ nm} CO + O(^1D)$	2.8×10^{-8}
$CO_2 + h\nu \xrightarrow{167 \leqslant \lambda \leqslant 216\ nm} CO + O$	6.4×10^{-9}
$CH_2O + h\nu \to CHO + H$	6.6×10^{-5}
$CH_2O + h\nu \to CO + H_2$	8.9×10^{-5}
$CH_4O_2 + h\nu \to CH_3 + OH$	7.1×10^{-5}

[a] For detailed data references and discussion, see Turco (ref. 65) and Turco and Whitten (ref. 19).

[b] Twenty-four hour average photodissociation rates at 120 km altitude are given.

TABLE 6.– PHOTOCHEMICAL REACTIONS AND RATE
COEFFICIENTS FOR CHLORINE COMPOUNDS

Reaction	Rate constant[a]	Note
$Cl + O_3 \rightarrow ClO + O_2$	$2.7 \times 10^{-11} e^{-257/T}$	
$Cl + CH_4 \rightarrow HCl + CH_3$	$7.3 \times 10^{-12} e^{-1260/T}$	
$Cl + H_2 \rightarrow HCl + H$	$3.5 \times 10^{-11} e^{-2290/T}$	
$Cl + HO_2 \rightarrow HCl + O_2$	3.0×10^{-11}	
$Cl + HNO_3 \rightarrow HCl + NO_3$	$1.0 \times 10^{-11} e^{-2170/T}$	
$Cl + H_2O_2 \rightarrow HCl + HO_2$	$1.7 \times 10^{-12} e^{-384/T}$	
$ClO + O \rightarrow Cl + O_2$	$7.7 \times 10^{-11} e^{-130/T}$	
$ClO + NO \rightarrow Cl + NO_2$	$1.0 \times 10^{-11} e^{200/T}$	
$ClO + O_3 \rightarrow ClO_2 + O_2$	$1.0 \times 10^{-12} e^{-4000/T}$	
$ClO + NO_2 + M \rightarrow ClONO_2 + M$		b
$ClONO_2 + O \rightarrow ClO + NO_3$	$3.0 \times 10^{-12} e^{-808/T}$	
$ClO + HO_2 \rightarrow HOCl + O_2$	2.0×10^{-13}	
$ClO_2 + O \rightarrow ClO + O_2$	$2.0 \times 10^{-11} e^{-1100/T}$	
$ClO_2 + NO \rightarrow ClO + NO_2$	$2.5 \times 10^{-12} e^{-600/T}$	
$ClO + ClO \rightarrow Cl + Cl + O_2$	$1.5 \times 10^{-12} e^{-1238/T}$	
$ClO + ClO \rightarrow Cl + ClO_2$	$2.1 \times 10^{-12} e^{-2200/T}$	
$Cl + ClO_2 \rightarrow ClO + ClO$	5.9×10^{-11}	
$HCl + OH \rightarrow Cl + H_2O$	$3.0 \times 10^{-12} e^{-425/T}$	
$HCl + O \rightarrow Cl + OH$	$1.1 \times 10^{-11} e^{-3370/T}$	
$HCl + O(^1D) \rightarrow Cl + OH$	1.4×10^{-10}	
$CF_2Cl_2 + O(^1D) \rightarrow ClO + Cl$	2.0×10^{-10}	
$CFCl_3 + O(^1D) \rightarrow ClO + Cl + Cl$	2.3×10^{-10}	
$CH_3Cl + OH \rightarrow Cl + CH_2$	$2.2 \times 10^{-12} e^{-1142/T}$	
$ClO + h\nu \rightarrow Cl + O$	2.8×10^{-3}	c
$ClO_2 + h\nu \rightarrow ClO + O$	1.6×10^{-1}	c
$ClONO_2 + h\nu \rightarrow ClO + NO_2$	5.6×10^{-4}	c
$HOCl + h\nu \rightarrow Cl + OH$	9.6×10^{-4}	c
$HCl + h\nu \rightarrow Cl + H$	1.6×10^{-6}	c
$CF_2Cl_2 + h\nu \rightarrow Cl + Cl$	1.3×10^{-6}	c
$CFCl_3 + h\nu \rightarrow Cl + Cl + Cl$	7.1×10^{-6}	c
$CH_3Cl + h\nu \rightarrow Cl + CH_3$	1.0×10^{-6}	c
$CCl_4 + h\nu \rightarrow Cl + Cl + Cl + Cl$	1.5×10^{-5}	c

[a]Rate constants are in molecule-cm-sec units. Unless otherwise noted, the rate constants are taken from Hudson (ref. 6).

[b]The expression adopted for this rate constant is given in Hudson (ref. 6).

[c]Twenty-four hour average photodissociation rates at 120 km altitude are given.

Another peroxy compound, peroxynitric acid (HO_2NO_2), has recently been proposed as a potentially important stratospheric constituent (refs. 71,72). Only the formation rate and thermal decomposition rate of HO_2NO_2 have been measured (refs. 66,71). Accordingly, we have omitted peroxynitric acid from our nominal SST calculations. However, we have included HO_2NO_2 for the purpose of a sensitivity study, giving it a photodissociation rate identical to that for H_2O_2 (ref. 72). Our results are discussed in section 4.

All of the peroxy compounds just mentioned (H_2O_2, CH_4O_2, HO_2NO_2) can react with OH. If peroxynitric acid happens to react rapidly with OH (by analogy with the OH + HO_2 reaction), this process could greatly limit the HO_2NO_2 concentration in the stratosphere and could also act as a strong sink for hydrogen radicals ($HO_X \equiv H + OH + HO_2$). We will see later that the abundance of HO_X in the lower atmosphere is a critical parameter in an SST assessment.

The photolysis of formaldehyde vapor (CH_2O) can lead to two sets of products: reactive radicals (H + HCO) and saturated molecules ($H_2 + CO$). The branching ratio between these products can affect the stratospheric concentration of HO_X. We have used the branching ratios of McQuigg and Calvert (ref. 73) for most of our calculations. G. K. Moortgat (private communication) has also measured the CH_2O photolysis products and quantum yields, and his results indicate a greater production of radical species. Figure 9 illustrates the differences between the two quantum yield measurements in terms of the number of hydrogen radicals that are generated by each methane molecule oxidized in the stratosphere (a com-

Figure 8.– Calculated hydrogen peroxide photodissociation rates and molecular concentrations in the stratosphere. Absorption cross sections are also shown.
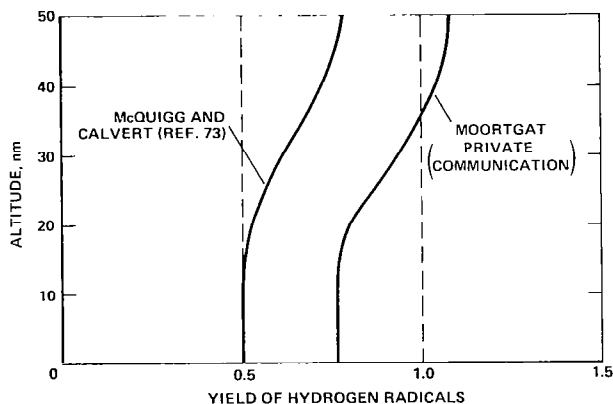
Figure 9.– Net yield of hydrogen radicals for each methane molecule oxidized in the lower atmosphere.

plete discussion of methane oxidation reactions is given later in this section). Curves are shown in figure 9 for two sets of formaldehyde quantum yield data, which are due to McQuigg and Calvert (ref. 73) and Moortgat (private communication). We will investigate the implications of these differences in section 4.
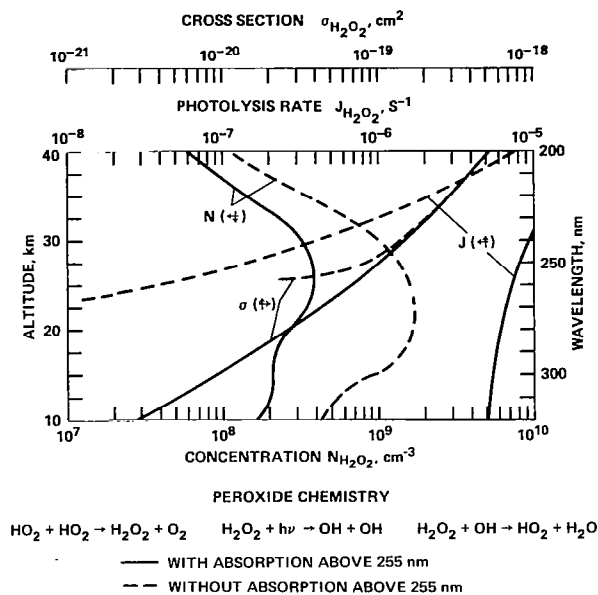
As we have already mentioned, diurnal variations are treated in our model by determining 24-hr average chemical rates and photodissociation coefficients for use in the species continuity equations. This scheme is described by Turco and Whitten (ref. 20) and in reference 9.

Effects of Recent Rate Coefficient Changes on Predicted Ambient Species Concentrations

Since the abundances of many of the trace constituents normally present in the atmosphere can influence the interaction of SST-injected nitrogen oxides with stratospheric ozone, it is useful to investigate the ways in which their predicted concentrations have changed as a result of recent rate coefficient modifications. For example, the calculated species concentrations shown in figures 5–7 have, in many instances, been affected significantly by the adoption of the fast Howard and Evenson (ref. 10) rate constant for reaction (2). Some of these changes are related to the corresponding increase in the calculated OH abundance shown in figure 6(a). Note, however, that even though the calculated OH abundance below 35 km has increased dramatically using the revised rate constant for reaction (2) the qualitative agreement between the model OH profile and the measured OH amount is not greatly affected. (OH measurements between 10 and 30 km are obviously needed to check this model result.) It should also be mentioned that between 30 and 40 km our latest prediction for the average daytime OH concentrations with the fast rate constant for reaction (2) are roughly twice as large as Anderson's measured values at a zenith angle of 80° (see fig. 6(a)). A comparison of Anderson's measurements with a computed diurnal variation for OH indicates that our current OH prediction is consistent with his data. However, because of the large OH variability which has been detected (e.g., ref. 51) the agreement of a model prediction with a single observed OH profile is certainly not a conclusive validation of the model result.

Calculated NO and NO_2 concentrations are reduced in our revised model because the enhanced OH abundance converts these species more efficiently into nitric acid. The ambient daytime ratio of HNO_3 to NO_2 in the model, which is about 13 at 20 km, is now much larger than the ratio of 1.5 to 4.0 near 20 km determined experimentally by Evans et al. (ref. 74); this fundamental disagreement has not yet been resolved. The $HNO_3:NO_2$ ratio in the lower stratosphere is a critical parameter for an SST assessment because NO_x emitted by aircraft engines will be partitioned in approximately the same way as ambient NO_y. It should be appreciated that an uncertainty in this ratio may be largely reflected in the calculations of the ozone perturbations caused by SST's. It is especially significant that the model $HNO_3:NO_2$ ratios are much larger than observed; it may mean that we are systematically underestimating ozone alterations due to SST's with current stratospheric models.

With the larger rate constant for reaction (2) the predicted ambient NO_2 abundance at 20 km is about one-half of that with the smaller rate constant. While the calculated NO profile is well within the limits of measurements, the NO_2 profile now appears to be somewhat low (see figs. 5(a) and (b)). The nitric acid distribution in the model is only in fair agreement with the observational data (fig. 5(c)). In fact, the HNO_3 predictions appear to be too large throughout the stratosphere, a problem which may be related to the large $HNO_3:NO_2$ ratios currently predicted by models.

The computed concentrations of $C\ell$ and $C\ell O$ are in better accord with the measurements of Anderson et al. (ref. 75) when the Howard and Evenson (ref. 10) rate coefficient for reaction (2) is used in a model. For example, figure 7(a) shows that with 3 ppbv of total chlorine ($C\ell_x$) in the

stratosphere, a $C\ell O$ profile lying roughly midway between the Anderson et al. (ref. 75) extreme observations, and with the same general shape, is now predicted. Compare the curve in figure 7(a) for 1.5 ppbv of $C\ell_x$ and the old rate coefficient of reaction (2); this result agrees only in shape with the lower limit of Anderson's values and has much too low a magnitude.

Observations of stratospheric $HC\ell$, shown in figure 7(b), are quite diverse. Several of the measurements indicate a sharp decrease in the mixing fraction of $HC\ell$ with increasing height in the middle stratosphere. This behavior is not predicted by theoretical models; almost without exception, calculated $HC\ell$ mixing fractions increase in magnitude monotonically with increasing height. The most recent spectroscopic data collected by Raper et al. (ref. 61) does show a steadily increasing $HC\ell$ mole fraction up to 40 km. In figure 7(b), calculated $HC\ell$ distributions corresponding to 1.5 and 3.0 ppbv of total stratospheric chlorine roughly bracket the measured values. To some degree the Howard and Evenson (ref. 10) rate constant measurement has allowed a greater quantity of stratospheric $C\ell_x$ to be used in model calculations and still be compatible with the $HC\ell$ observations.

In figure 7(c) the new model prediction for the chlorine nitrate concentration profile using a large rate coefficient for reaction (2) lies somewhat above the new upper limit for $C\ell ONO_2$ reported by Murcray et al. (ref. 62). The average chlorine nitrate concentration between 10 and 30 km, however, is roughly within Murcray's limiting value. It should be pointed out that the existing measurements of $HC\ell$ and $C\ell ONO_2$ also appear to restrict the total amount of stratospheric chlorine that can be realistically included in a model using current photochemistry to about 2−3 ppbv; in our model, the ambient $C\ell_x$ mixing ratio turns out to be about 2 ppbv (including about 1 ppbv due to $CH_3C\ell$).

Aeronomic Perturbations Caused by Aircraft Exhaust Emissions of NO_x

In the present calculations of aircraft perturbations, we inject SST NO_x as NO and distribute it uniformly over the globe in a 2-km-thick spherical shell centered in altitude at the assumed height of SST flight (the vertical grid spacing in our numerical model is 2 km); for a fleet of planes, an equivalent global NO_x emission rate in kg of NO_2/yr is easily converted into a local NO injection rate in molecules per cubic meter per second for the spherical shell.

Nitrogen oxides from aircraft engines are usually released as a mixture of NO and NO_2. The $NO:NO_2$ ratio in the aircraft wake rapidly adjusts to the ratio in the local ambient environment with the liberation or consumption of a small, and usually negligible, amount of odd oxygen $[O + O_3 + O(^1D)]$ (from an aeronomical point of view, the NO_2 molecule is a weakly bound combination of the species NO and O; i.e., it contains one unit of odd-oxygen). Actually, our assumption that pure NO is emitted from SST engines is probably very close to reality (ref. 4).

Nitrogen oxides introduced by SST traffic at high altitude add to the ambient background level of NO_y, which is generated principally by the chemical decomposition of N_2O by $O(^2D)$ atoms between 30 and 40 km. (In our model we also include nitrogen oxide production by cosmic rays in the lower stratosphere (ref. 76) and by ionospheric processes in the upper mesosphere (ref. 77). However, both of these NO_y sources are negligible compared to the N_2O source.) Injected nitrogen oxides will interact with ozone and other air constituents to alter the characteristics of the

stratosphere. Crutzen (ref. 78) and Johnston (ref. 79) have shown that ozone is very efficiently destroyed by the NO_x catalytic cycle

$$O_3 + NO \rightarrow O_2 + NO_2 \tag{3}$$

$$O + NO_2 \rightarrow O_2 + NO \tag{4}$$

$$O + O_3 \rightarrow 2\,O_2 \qquad \text{(overall reaction)}$$

which in our model is about four times as effective as the direct odd-oxygen loss reaction

$$O + O_3 \rightarrow 2\,O_2 \tag{5}$$

It is the reaction of NO_2 with atomic oxygen that limits the rate of decomposition of ozone by NO_x in the stratosphere, because NO_2 can, alternatively, be rapidly recycled into ozone,

$$NO_2 + h\nu \rightarrow NO + O \tag{6}$$

$$O + O_2 + M \rightarrow O_3 + M \tag{7}$$

At stratospheric altitudes the O to O_3 concentration ratio is determined mainly by reaction (7) in competition with ozone photolysis.

Not all of the NO_x emitted by SST's actually participates in the ozone destruction cycle; a large part of it is stored as inert nitric acid vapor through the reaction

$$NO_2 + OH + M \rightarrow HNO_3 + M \tag{8}$$

Nitric acid can accumulate to large amounts in the lower stratosphere because its loss mechanisms (photolysis and reaction with OH) are relatively inefficient, especially in the lower stratosphere. Some of the active nitrogen, NO_x, can also be stored as N_2O_5 and $ClONO_2$ in the stratosphere through the reactions

$$NO_2 + O_3 \rightarrow NO_3 + O_2 \tag{9}$$

$$NO_2 + NO_3 + M \rightarrow N_2O_5 + M \tag{10}$$

$$NO_2 + ClO + M \rightarrow ClONO_2 + M \tag{11}$$

For present-day stratospheric conditions, however, our model shows that the concentrations of N_2O_5 and $ClONO_2$ together are only about 10% to 20% of the HNO_3 concentration, and therefore represent only a small secondary reservoir for NO and NO_2 (the case when large chlorine abundances may significantly boost the $ClONO_2$ component is treated in this assessment only by way of a sensitivity calculation).

In our calculations, nitrogen oxides deposited in the stratosphere evolve in a specific way. First, some of the added NO and NO_2 is partially transformed by photochemistry into other NO_y

compounds (e.g., N, NO_3, N_2O_5, HNO_2, HNO_3, $C\ell ONO_2$). Below 30 km, the largest fraction becomes nitric acid. The remaining NO and NO_2 catalytically attack ozone. Slowly, NO_y is mixed downward into the troposphere where it is quickly removed from the air by washout and rainout processes.

A smaller amount of the NO_y is transported to altitudes above 30 km, where NO is the predominant odd-nitrogen compound; eventually NO reaches the upper stratosphere and lower mesosphere (between ~35 and ~75 km) where there is an active photochemical sink (e.g., see refs. 17,80)

$$NO + h\nu \rightarrow N + O \tag{12}$$

$$NO + N \rightarrow N_2 + O \tag{13}$$

In our model, we find that about 40% of the upward-diffusing NO_y is actually destroyed in the mesosphere. Duewer et al. (ref. 80) have demonstrated that the height profiles of both ambient and SST-injected nitrogen oxides are strongly affected by NO photolysis at high altitudes, even though these workers have truncated their model near the stratopause and appear to have neglected a large portion of the photolysis sink in their calculations.

There are other important photochemical processes involving NO_x compounds which serve to counter their destruction of ozone in the stratosphere. Before considering these processes, however, we will discuss the reactions of hydrogen and hydrocarbon compounds which can also affect ozone abundances.

The Photochemistry of Hydrogen Radicals and Water Vapor Emitted by Aircraft

In the lower stratosphere, hydrogen radicals catalytically destroy ozone molecules through the reaction sequence,

$$OH + O_3 \rightarrow HO_2 + O_2 \tag{14}$$

$$HO_2 + O_3 \rightarrow OH + 2\,O_2 \tag{15}$$

$$\overline{}$$

$$2\,O_3 \rightarrow 3\,O_2 \qquad \text{(overall reaction)}$$

(a similar description of HO_x catalysis is presented by Johnston and Nelson (ref. 81)). At higher altitudes, odd-oxygen is consumed by the processes

$$OH + O \rightarrow H + O_2 \tag{16}$$

$$H + O_2 + M \rightarrow HO_2 + M \tag{17}$$

$$HO_2 + O \rightarrow OH + O_2 \tag{18}$$

$$\overline{}$$

$$O + O \rightarrow O_2 \qquad \text{(overall reaction)}$$

and

$$OH + O \rightarrow H + O_2 \tag{16}$$

$$\underline{H + O_3 \rightarrow OH + O_2} \tag{19}$$

$$O + O_3 \rightarrow 2\,O_2 \qquad \text{(overall reaction)}$$

Reaction (17) is also an important step in some photochemical smog mechanisms (see below). Interestingly, reaction (2) — followed by reactions (6) and (7) — interferes with HO_X ozone destruction by effectively competing with catalytic steps (15) and (18); thus the reaction of NO with HO_2 acts to short-circuit ozone consumption by hydrogen compounds.

Hydroxyl and hydroperoxyl (HO_2) radical concentrations are generated by the reaction of water molecules with excited oxygen atoms (produced by ozone photolysis in the Hartley band)

$$O(^1D) + H_2O \rightarrow 2\,OH \tag{20}$$

and by methane oxidation (see the following subsection for a detailed discussion of methane chemistry). The concentration ratio of OH to HO_2 below 30 km is largely controlled by reactions (2) and (14).

All of the hydrogen radicals (HO_X) can recombine with one another to form H_2 and H_2O along several paths, the most important of which is the reaction

$$OH + HO_2 \rightarrow H_2O + O_2 \tag{21}$$

Hydrogen peroxide, a product of the association reaction

$$HO_2 + HO_2 \rightarrow H_2O_2 + O_2 \tag{22}$$

can be formed in relatively large amounts in the stratosphere because of its small photolysis rate and low reactivity (see fig. 8). Hydrogen peroxide (along with related molecules such as CH_4O_2 and HO_2NO_2) can limit the total abundance of hydrogen radicals in stratospheric air via hydrogen abstraction reactions; for example,

$$OH + H_2O_2 \rightarrow H_2O + HO_2 \tag{23}$$

Another important HO_X sink is the reaction

$$OH + HNO_3 \rightarrow H_2O + NO_3 \tag{24}$$

which can also generate a small amount of odd-oxygen if NO_3 is photolyzed into NO_2 and O, and can — in extreme cases — limit the formation of nitric acid. Reaction (24) is especially important when NO_y concentrations are enhanced by SST NO_X emissions. In this case, increased HNO_3 abundances can make reaction (24) surpass reaction (21) as the dominant HO_X sink in the lower stratosphere.

Water vapor is a major component of aircraft exhaust, and for some of our calculations we have injected it into the stratosphere along with NO_X at a rate determined by its emission index of 1.3 kg H_2O/kg fuel (ref. 4, monograph 2). For an assumed NO_2 emission index of 6 g NO_2/kg fuel,

24

about 550 H_2O molecules are injected with each NO_x (or NO) molecule. Many previous studies of SST effects have only partially treated water vapor injection. In the present situation, however, revised photochemistry leads to much smaller SST/NO_x-induced ozone reductions and amplifies the role of HO_x chemistry in the stratospheric ozone budget. By reducing the NO_x component in SST exhaust, advanced engine technology will lead to larger H_2O:NO_2 emission ratios, and water vapor effects may become quite important in comparison to NO_x effects. In fact, we show later that, because of its chemical activity, the water vapor injected by SST's can cause net stratospheric ozone reductions. Nevertheless, because of the unresolved issue of water vapor temperature feedback effects (discussed earlier), we have made SST calculations both with and without water vapor release.

Methane Oxidation and Its Effects

Below 30 km, an important hydroxyl radical reaction is

$$OH + CH_4 \rightarrow H_2O + CH_3 \tag{25}$$
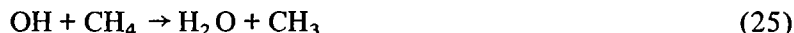
Reaction (25) both destroys odd-hydrogen and initiates the methane oxidation chain which eventually generates HO_2, H_2, and carbon monoxide among other products. Figure 10 gives a schematic representation of the methane oxidation r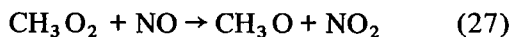eactions included in our model; rates for each of the individual photochemical processes can be found in tables 4 and 5. In general, reaction (25) eventually produces more HO_x — mainly in the form of HO_2 — than it destroys. Moreover, methane decomposition in the lower stratosphere leads to ozone production via a photochemical mechanism similar to that occurring in polluted urban atmospheres. The yields of odd-oxygen and odd-hydrogen production and loss at each reaction step, and their net production for the entire sequence are also indicated in figure 10.

One component of the methane smog mechanism involves the methyl radicals produced by reaction (25). These radicals react rapidly to form a peroxy compound,

$$CH_3 + O_2 + M \rightarrow CH_3O_2 + M \tag{26}$$

which then reacts with NO as discussed previously,

$$CH_3O_2 + NO \rightarrow CH_3O + NO_2 \tag{27}$$

Reaction (27) followed by reactions (6) and (7) generates ozone.

OXYGEN*   HYDROGEN

OXYGEN*		HYDROGEN
0	CH_4 → OH	-1
0	CH_3 → O_2	0
$f_1 \cdot f_3$	$f_1^\dagger$ CH_3O_2 f_3 NO HO_2 OH CH_4O_2	$-2(f_3 - f_2)$
	f_2 $h\nu$	
$+1$	CH_3O → O_2	$+1$
g_2	$g_1^\dagger$ CH_2O g_3 g_2 $h\nu$ OH	$g_2 - g_3$
$g_2 + g_3$	$h\nu$ CHO → O_2	$g_2 + g_3$
$+1$	CO → OH	0
	CO_2	
$2 + f_1 - f_3 + 2g_2 + g_3$	NET	$2g_2 - 2(f_3 - f_2)$
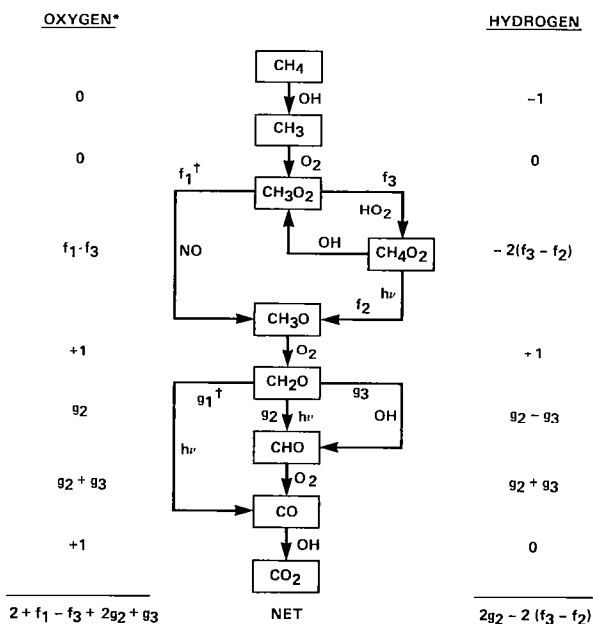
* Fractional numbers of atoms generated for each methane molecule oxidized. To obtain these fractions, unit efficiency is assumed at each step of the related chemical chain:

$$H \xrightarrow{O_2} HO_2 \xrightarrow{NO} NO_2 \xrightarrow{h\nu} O \xrightarrow{O_2} O_3$$
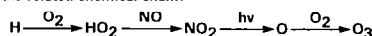
† The f's and g's are branching ratios; branch f_3, however, is normalized relative to $f_1 + f_2 = 1$.

Figure 10.— Methane oxidation sequence in the lower stratosphere.

The concentration of CH_3O_2 is limited mainly by reaction (27). However, CH_3O_2 can also react with HO_2,

$$CH_3O_2 + HO_2 \rightarrow CH_4O_2 + O_2 \qquad (28)$$

The CH_4O_2 molecules that are formed may be photolyzed into CH_3O and OH (products analogous to H_2O_2 photodissociation fragments) short-circuiting ozone production by reaction (27), or they may react with OH, reducing odd-hydrogen concentrations. However, because of recent kinetic rate data revisions, such CH_4O_2 effects turn out to be quite small.

Another important factor in methane oxidation chemistry is the branching ratio for the production of radicals (H and CHO) and molecules (H_2 and CO) in the photolysis of formaldehyde. In our nominal calculations, we have used the quantum yield data of McQuigg and Calvert (ref. 73) which is the only complete set of data appropriate for stratospheric pressures. However, we have also studied the implications of adopting the quantum yield data recently obtained by Moortgat (private communication). For example, figure 9 compares the effect of these two data sets on the predicted net production of HO_X during methane oxidation.

The CO that is liberated by formaldehyde decomposition, together with CO that is transported upward from the troposphere, can react further with OH,

$$OH + CO \rightarrow H + CO_2 \qquad (29)$$

Reaction (29), followed by reactions (17), (2), (6), and (7) also generates some ozone in the lower stratosphere.

Although the methane smog reactions are particularly important in evaluating ozone alterations due to subsonic aircraft flying at relatively low altitudes, they are also important in SST calculations. Our recent model studies, and those of other workers, indicate that SST's flying as high as 20 km altitude can lead to a net stratospheric ozone column increase (e.g., ref. 22); part of this increase is due to smog reactions.

Summary of the Importance of the $NO + HO_2$ Reaction and Related Processes

Returning to the discussion of NO_X interactions with other stratospheric constituents, the process

$$NO + HO_2 \rightarrow NO_2 + OH \qquad (2)$$

with a fast kinetic rate coefficient can be seen to have at least three important implications:

1. By superseding HO_2 reaction (15), reaction (2) — together with reaction (14) — determines the $OH:HO_2$ concentration ratio in the lower stratosphere and, because it is fast, leads to a substantial increase in the calculated OH abundances below 30 km. An enhanced OH level has several important consequences:

a. Increased OH reduces the NO and NO_2 concentrations by converting these gases into HNO_3 through reaction (8).

b. Increased OH amplifies the oxidation rate of methane and CO by reactions (25) and (29), thereby generating HO_2 and ozone more rapidly. The rate of methane destruction by reaction (25) also affects the predicted vertical profile of CH_4 in the stratosphere, with implications for simulated vertical transport rates.

c. Increased OH accelerates the rate of conversion of stable hydrogen chloride gas, $HC\ell$, into ozone-destructive chlorine oxides, $C\ell$ and $C\ell O$ (see the discussion below).

d. Increased OH augments the losses of HO_x by recombination through reactions (21) to (24). However, part of this increased loss rate is offset by an increased production rate of HO_x due to methane oxidation.

2. A rapid interaction between NO and HO_2 allows most of the HO_2 formed during the CH_4 and CO oxidation sequences to form ozone (by reactions (2), (17), (6), and (7)) rather than react with and destroy ozone (reaction (15)). The efficiency of ozone-generation by smog chemistry is therefore greatly enhanced; in fact the efficiency becomes almost unity in the lower stratosphere (i.e., for each peroxy molecule that is formed, an ozone molecule is generated).

3. A rapid reaction between NO and HO_2 short-circuits the catalytic destruction of ozone by HO_x reactions (15) and (18). Nonetheless, the catalytic activity of ambient HO_x is increased relative to that of ambient NO_x in the lower stratosphere. This shift in catalytic activity means, for one thing, that SST-added water vapor can now react chemically to reduce stratospheric ozone.

When nitrogen oxides are injected into the stratosphere, HO_x recombination is accelerated (particularly by reaction (24)) and HO_x concentrations are decreased. In addition, HO_2 is recycled more rapidly into OH. As a result, the rate of destruction of ozone by HO_x is reduced and the fractional amount of ozone-active NO_x (relative to ozone-inert HNO_3) may be increased, depending upon the absolute change in the OH concentration. When water vapor is also added, however, HO_x concentrations are reduced much less, and methane oxidation may be accelerated. Obviously, consideration of all the NO_x-HO_x interactions related to SST perturbations is quite involved, more so because the relative importance of these interactions depends upon the level of NO_x injection and the treatment of water vapor emission. Even so, one can obtain a reasonable understanding of these coupled photochemical processes by applying the basic aeronomical principles outlined above.

Effects of Chlorine Chemistry

Nitrogen oxides interact with chlorine constituents and form chlorine nitrate by reaction (11); chlorine nitrate is an additional atmospheric reservoir for NO_x as well as one for chlorine. Chlorine nitrate aeronomy has been discussed at length in the National Academy of Sciences (ref. 3), and by Rowland et al. (refs. 82,83). To a first approximation, chlorine nitrate concentrations below 30 km are proportional to the NO_2:NO abundance ratio. (This is so because the $C\ell ONO_2$ production rate is proportional to the NO_2-$C\ell O$ concentration product, the $C\ell O$ abundance is (roughly) inversely proportional to the NO concentration (below 30 km), and the $C\ell ONO_2$ loss rate is fixed (by

photolysis).) Therefore, we expect chlorine nitrate concentrations to be relatively insensitive to (small) NO_x injections; this conjecture is borne out by our detailed calculations.

As noted earlier, reaction (2) is also coupled into the NO_x-$C\ell_x$ chemical sequence. An increase in NO_x affects the OH concentration thereby affecting the production rate of chlorine atoms through the decomposition of $HC\ell$ in the reaction

$$OH + HC\ell \rightarrow H_2O + C\ell \qquad\qquad (30)$$

The chlorine atoms released by reaction (30) catalyze ozone destruction through the kinetic cycle (e.g., refs. 84,85),

$$O_3 + C\ell \rightarrow O_2 + C\ell O \qquad\qquad (31)$$

$$O + C\ell O \rightarrow O_2 + C\ell \qquad\qquad (32)$$

$$\overline{}$$

$$O + O_3 \rightarrow 2\, O_2 \qquad\text{(overall reaction)}$$

In the first reaction step, $C\ell O$ is formed and, as already mentioned, it may combine with NO_2 to form chlorine nitrate.

Normally, another NO_x-$C\ell_x$ reaction, namely,

$$NO + C\ell O \rightarrow NO_2 + C\ell \qquad\qquad (33)$$

strongly moderates the chlorine-sensitized destruction of ozone by regenerating some odd-oxygen via NO_2 and reactions (6) and (7). As NO is increased, therefore, ozone decomposition by chlorine oxides is reduced.

Reaction (33) also acts to increase the ambient stratospheric NO_2:NO concentration ratio (to a degree that is dependent upon the $C\ell_x$ level), thus leading to more effective odd-oxygen destruction by a fixed amount of NO_x. In our ambient model atmosphere, for example, the increase in the NO_2:NO ratio is about 20% of the value which would be due to the ozone reaction (3) alone.

It is noteworthy that the increase in the rate constant for reaction (2) has increased the ozone activity of $C\ell_x$, while it has decreased that of NO_x. In fact, in changing from the old to the new (larger) rate coefficient for reaction (2), chlorine catalysis of ozone has become nearly twice as effective as before. Even so, for the small ambient amounts of chlorine in our present model, and those projected for the near future, $C\ell_x$-NO_x interactions still have less importance for SST calculations than do NO_x-HO_x interactions.

## 4. RESULTS OF SST SIMULATIONS

As we have already mentioned in the preceding section, the ozone balance in the SST perturbed stratosphere is affected by several competing reaction sequences: the NO_x, HO_x, and

$C\ell_X$, catalytic cycles normally cause ozone losses, but the methane smog sequence causes an ozone gain. For small NO_X injections by SST's, our model results suggest that NO_X consumption of ozone is increased, but HO_X destruction of ozone is decreased to a greater degree; in addition, $C\ell_X$ ozone consumption is reduced somewhat and methane oxidation is accelerated slightly. When all of these effects are combined, stratospheric ozone shows a small net increase as we will show below. As the NO_X injection rate is made larger, HO_X concentrations are depressed to the point where the methane oxidation rate begins to decrease and, more importantly, the concentrations of NO and NO_2 relative to HNO_3 begin to increase; for large NO_X injection rates there is a net destruction of ozone, which results primarily from the increasing efficiency of NO_X catalysis.

Calculated Stratospheric Ozone Perturbations

We have calculated steady-state ozone column changes for a wide range of SST NO_X injection rates, at several assumed flight altitudes, using the WT, DC, and HN diffusion profiles; the results are shown in figures 11(a) and (b), and 12. Our method for including SST NO_X (and H_2O) emissions in model computations has been discussed in section 3. Figure 11(a) given the percentage change in the total stratospheric ozone column abundance as a function of the global injection rate of NO_X (in terms of the equivalent mass of NO_2) or H_2O at 20 km for all three eddy diffusion profiles.

The NO_X and H_2O injection rate scales in figure 11 correspond to an engine emission index ratio of 6 g NO_2/kg fuel and 1.3 kg H_2O/kg fuel, respectively (far-term engine technology and high NO_X case — see table 1). For NO_X injection, results are given for WT, DC, and HN diffusion profiles,
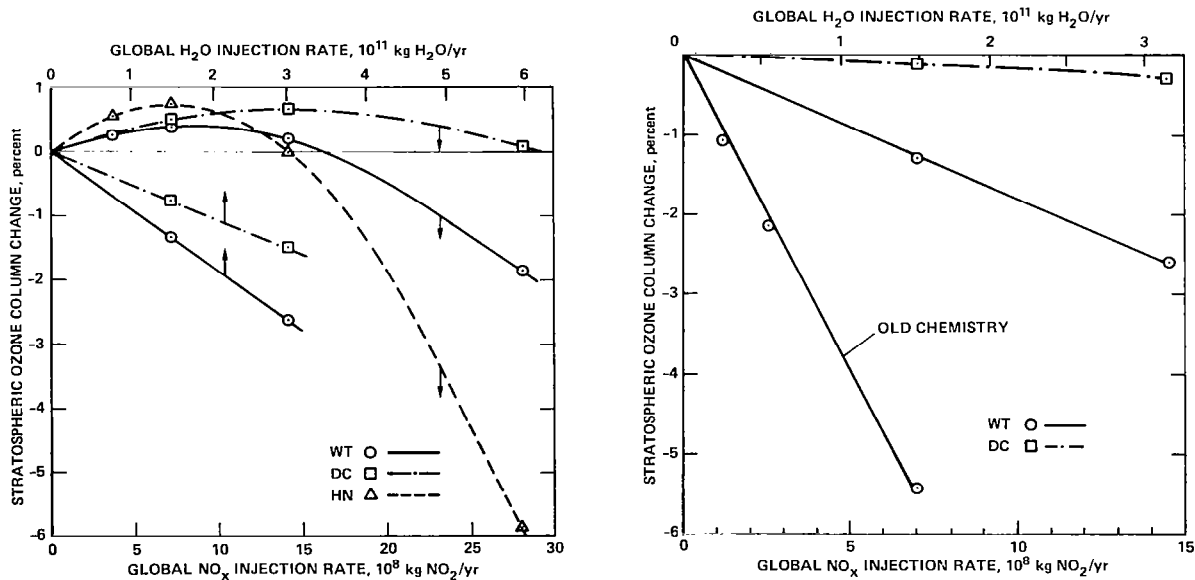
(a) As a function of the global injection rate of NO_X or H_2O at 20 km altitude.

(b) As a function of the simultaneous injection of NO_X and water vapor at 20 km altitude.

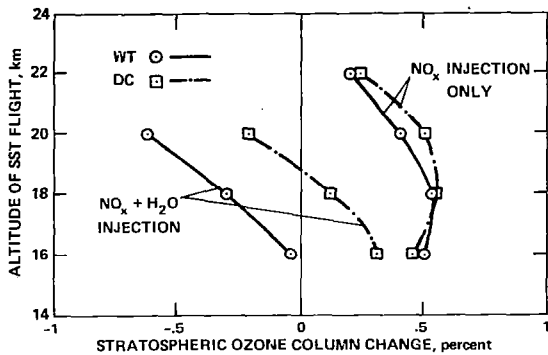Figure 11.— Calculated steady-state ozone column changes above 10 km.

Figure 12.– Calculated steady-state ozone column changes (above 10 km) as a function of altitude of injection of 7×10^8 kg NO_2/yr spread uniformly over the globe.

whereas for water vapor, injection results are shown only for the WT and DC diffusion profiles. Computed ozone changes are indicated by symbols, the curves interpolated between these points. The "old chemistry" curve in figure 11(b) is typical of advanced-SST ozone reduction estimates made prior to January 1977. The reader is warned that the curves corresponding to simultaneous emission of NO_X and H_2O can be used for the case of *6 g NO_2/kg fuel only*. The results for each diffusion coefficient show some similarities, and some differences. The basic disparities arise from differences in the effective stratospheric residence time (for injected gases) simulated by each diffusion coefficient. The HN, WT, and DC diffusivities yield (in that respective order) decreasing residence times for, and smaller accumulations of, injected pollutants.

Thus, for an aircraft fleet operating in the stratosphere, the HN diffusion profile leads to the largest ozone column effects, both enhancements and depletions (for a range of NO_X injections), while the DC profile leads to the smallest effects; the WT profile gives ozone column change lying between these two values.

In some earlier studies of SST effects (e.g., ref. 4, vol. 3), the injection of water vapor by high-flying aircraft was found to lead to small ozone increases in model calculations, while injected NO_X led to substantial ozone reductions; the added H_2O increased OH abundances and, by reaction (8), decreased the fractional amount of ozone-active nitrogen oxides in the air (see point 1(a), section 3).

However, when the new (larger) rate coefficient for reaction (2) is employed in a model, HO_X catalysis in the lower stratosphere increases in importance relative to NO_X, and the reaction sequences (14)–(15) and (16)–(18) become the dominant odd-oxygen destruction mechanisms (point 3, section 3). In this situation, stratospheric ozone will be reduced by water vapor injection. The data in figure 11(a) show that water vapor, injected alone, leads to substantial ozone column depletions; the ozone depletion varies almost linearly with the H_2O injection rate, at least for the range of injection rates used for the calculations shown in figure 11(a). The effect on ozone of H_2O injection can be compared with the effect of NO_X injection by noting that the H_2O and NO_X results in figure 11(a) correspond to the same number of aircraft when an NO_X emission index of 6 g NO_2/kg fuel is assumed. In calculating water vapor effects, we have omitted the HN vertical transport simulation because we have found that it leads to predictions of ozone change that are only slightly larger than those obtained with the WT diffusivity profile.

When H_2O and NO_X are injected together, their chemical cycles interact with one another such that *the net ozone change is somewhat less than the sum of the ozone changes calculated separately for each cycle* (see fig. 11(b)). The results given in figure 11(b) clearly indicate that advanced SST flights at 20 km could result in a net stratospheric ozone reduction due to the photochemical reactivity of the NO_X and H_2O in the exhaust emissions. In this case, the WT diffusion coefficient gives much larger ozone reductions than the DC diffusion coefficient, for reasons already discussed.

30

Figure 12 illustrates the stratospheric ozone column change as a function of the cruise altitude of a large fleet of SST's, both with and without the possible effect of water vapor. The fleet used for these calculations consists of 1200 baseline aircraft with far-term high NO_x emission indexes (or, equivalently, about 460 aircraft with near-term NO_x emission indexes). The corresponding NO_x emission rate is 7×10^8 kg NO_2/yr worldwide. This large emission rate has been utilized in making several of the figures in this report in order to produce ozone changes large enough to illustrate clearly the important SST effects. Results are given in figure 12 for WT and DC diffusion profiles. Also shown are several calculations in which water vapor is released along with nitrogen oxides; the rate of water vapor release, 1.5×10^{11} kg/yr, pertains to an NO_x engine emission index of 6 g NO_2/kg fuel, or far-term technology and high NO_x case (see table 1). Computed ozone changes are indicated by symbols with curves interpolated between these points. The general altitude dependence of the ozone column change is quite different from that reported earlier in the Department of Transportation reports (ref. 4, vol. 3).

When NO_x emissions are considered apart from other exhaust emissions, ozone column *increases* are predicted for SST flight at altitudes up to 22 km for both the WT and DC diffusion coefficients. Although the ozone enhancements shown in figure 12 are similar for the two diffusion coefficients, this situation does not hold for all NO_x injection rates (see fig. 11(a)). When water vapor emissions are included in the calculation, small ozone column decreases are predicted for 20 km SST operation. For operating altitudes as low as 16 km the situation is less clear, and ozone may be reduced or enhanced, depending upon the transport parameterization which is utilized (see fig. 12).

The diminishing effect of SST traffic on ozone with decreasing flight altitude below about 18 km (fig. 12) is due largely to the corresponding decrease in the stratospheric residence times of the injected exhaust gases, which limits their buildup above the tropopause. For SST flight above 18 km, greater amounts of injected NO_x and H_2O can reach the photochemically active region in the middle stratosphere where they efficiently destroy ozone; in fact the injection of NO_x or H_2O at a high enough altitude will always reduce ozone. In figure 13(a) we illustrate this point by showing the predicted absolute change in the ozone concentration profile due to an NO_x injection of 7×10^8 kg NO_2/yr (globally averaged) at 20 km; results are given for the WT and DC diffusivities with and without water vapor effects. (In the model, an equivalent number of NO molecules is actually injected.) The water vapor emission rate is taken to be 1.5×10^{11} kg of H_2O/yr, which pertains to an NO_x engine emission index of 6 g NO_2/kg fuel, or the far-term technology and high NO_x case in table 1. The corresponding relative (percent) change in the ozone concentration profile is shown in figure 13(b).

Note that ozone increases occur predominantly below 25 km, where one-dimensional model simulations are the most uncertain. At higher altitudes there is a clear-cut reduction of ozone in the region where O_3 is controlled by photochemical processes (those discussed in section 3). The injection of water vapor into the stratosphere moves the ozone perturbation curves in figures 13(a) and (b) to the left at all heights, demonstrating its strong photochemical effect on ozone abundances (in current model simulations).

Another interesting feature of figure 13(b) is the relatively large *local* ozone changes (up to 10 times as large as the total ozone column changes) due to SST operations. If ozone variations of this magnitude can affect atmospheric dynamic stability, then the modification of the ozone profile by SST's may turn out to be more important than the integrated ozone column change.
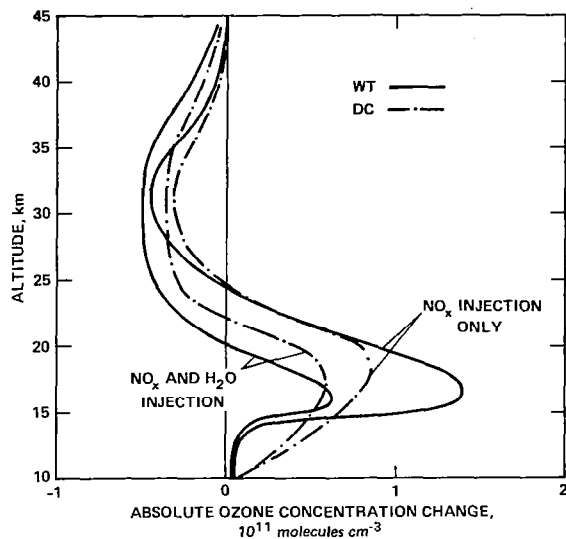
(a) Absolute change.
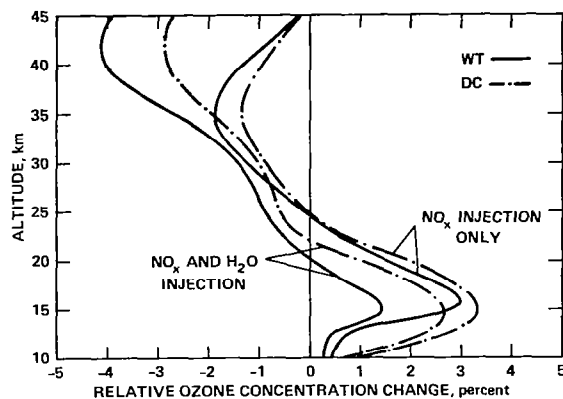
(b) Relative change.

Figure 13.— Calculated ozone concentration changes for a global NO_x injection rate of 7×10^8 kg NO_2/yr at 20 km.

Figure 14 shows the calculated absolute and relative changes in total stratospheric NO_y for a global NO_x injection rate of 7×10^8 kg NO_2/yr at 20 km. (This is the SST injection case considered in figures 13(a) and (b).) Two interesting effects are apparent: (1) for the WT diffusion profile there is a large NO_y buildup between the injection height and the tropopause, while for the DC diffusion coefficient the injected NO_y is concentrated closer to the height of injection because the height of the diffusion minimum coincides with the injection altitude; (2) for both profiles, the mixing ratio gradient of NO_y, which determines the direction of its net flow, is toward the troposphere below the injection height and toward the mesosphere above the injection height. The latter gradient, which is due to the NO photolysis sink above 35 km (see section 3), reduces significantly the amount of NO_y (and the related ozone depletion) in the photochemically active region above 30 km — well below that which would be predicted if the photolysis sink were ignored.

It has been suggested that SST flight altitudes assumed for one-dimensional model calculations should be adjusted upward by about 2 km to account for the difference between the actual height that SST's fly above the tropopause level in high latitude traffic lanes, and the height simulated
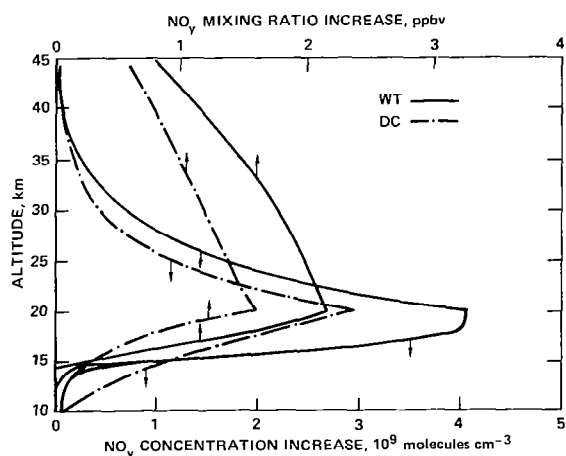

Figure 14.— Calculated absolute and relative changes in total stratospheric NO_y for a global injection rate of 7×10^8 kg NO_2/yr at 20 km.

in most 1-D models (e.g., ref. 86). For the traffic patterns developed for use in our 2-D model studies (to be presented in a subsequent report), we have found that a 13 km mean "tropopause" height is appropriate.

Sensitivity Tests for Aircraft Effects

In order to investigate the nature of some of the chemical interactions occurring in the stratosphere, and their influence on calculated ozone reductions by high-flying aircraft, we have performed several sensitivity tests with our model. For each sensitivity calculation a single model parameter has been altered, a new ambient atmosphere determined, and an SST-NO_x ozone perturbation computed. Only the WT diffusion coefficient has been used in the sensitivity analysis, and 20 km SST flight has been assumed. The results of the tests are summarized in table 7.

Most of the sensitivity calculations can be understood, at least semiquantitatively, in terms of the relative magnitudes of the NO_x, HO_x, and $C\ell_x$ ozone-catalytic cycles, and the degree of interaction between these cycles. For example, added NO_x reduces the catalytic activity of both HO_x and $C\ell_x$: the former because the $NO + HO_2$ reaction short-circuits ozone destruction by HO_x while the $HNO_3 + OH$ reaction reduces total HO_x; the latter because the $NO + C\ell O$ reaction limits the rate of odd-oxygen consumption by $C\ell_x$. Other less important interactions also occur; the discussion in section 3 gives a more complete description of these secondary processes.

It has been proposed that N_2O production due to fertilizer denitrification could accelerate dramatically in future decades (ref. 87), and that increased atmospheric N_2O concentrations could follow (ref. 88). As N_2O abundances increase, so do stratospheric NO_y concentrations. Against such

TABLE 7.— SENSITIVITY STUDIES OF OZONE PERTURBATIONS DUE TO SST's[a]

Model modification	Stratospheric ozone column changes due to SST NO_x injection[b]	
	Without water vapor effect	With water vapor effect
Increase background N_2O by 50%	-0.35%	-0.88%
Increase total chlorine to 5 ppbv	2.13%	.42%
Eliminate chlorine nitrate formation	.80%	-.81%
Eliminate scattered radiation	.55%	-.54%
Eliminate diurnal effects	.30%	-.50%
Use Moortgat CH_2O quantum yields	.68%	-.38%
Include HO_2NO_2 formation	.17%	-.74%
Decrease the $HO_2 + O_3$ rate by a factor of 3	-.50%	-1.10%
Increase the $HO_2 + O_3$ rate by a factor of 3	1.80%	.13%
Increase the $OH + HNO_3$ rate by a factor of 3	-1.74%	-1.90%
Decrease ambient H_2O from 4.0 to 2.5 ppmv at 14 km	-.07%	-1.10%

[a] A global NO_x injection rate of 7×10^8 kg NO_2/yr, and the WT diffusion coefficient have been used for each sensitivity test.

[b] For reference, the nominal ozone column changes are +0.40% with the water vapor effect and -0.62% with it.

a rising background level of NO_y, a fixed (low level) emission rate of NO_x by SST engines becomes increasingly more efficient in consuming stratospheric ozone. At first, the ozone increase (if any) due to this fixed SST-NO_x injection becomes steadily smaller, and eventually an ozone reduction occurs. For a sensitivity test we have increased the ambient concentration of N_2O in our model simulation by 50%, which increases ambient NO_y by about the same amount. The data in table 7 indicate that, against this enhanced background of ambient nitrogen oxides, SST-NO_x emissions can now reduce ozone by a small quantity. The effect is due mainly to an increase in the importance of the NO_x catalytic reaction cycle compared to the HO_x cycle in the lower stratosphere as ambient NO_x accumulates there.

Aircraft exhaust effects on ozone column densities are found to be quite sensitive to the ambient concentration of atmospheric chlorine. The data in table 7 show that with 5 ppbv of $C\ell_x$ in the stratosphere (an increase of about 3 ppbv over the nominal amount in our model) SST flight at 20 km can result in a large ozone column increase of more than 2% (for the nominal fleet of planes). In another sensitivity test using a model with our assumed ambient 2 ppbv of stratospheric chlorine, but without chlorine nitrate formation, the ozone column increase due to SST-NO_x injection at 20 km is roughly twice that for the case when chlorine nitrate formation is included. In both of the chlorine sensitivity tests just mentioned, the role of $C\ell_x$ catalysis in the stratospheric ozone budget is enhanced. Thus, the interaction between added NO_x and ambient $C\ell_x$ is similarly enhanced, which results in a greater moderation of ozone depletion by $C\ell_x$. According to figure 14, the SST NO_x-ambient $C\ell_x$ interaction would be even more intense were it not for the falloff in the NO_y mixing ratio profile with increasing height between 30 and 40 km due to the NO photolysis sink above 40 km.

The present amount of chlorine in the atmosphere is not well established. Moreover, projections of large future increases of $C\ell_x$ due to chlorofluoromethane release are now questionable because of pending legislative restrictions on their commercial uses. Accordingly, our SST ozone perturbation calculations, which are based upon 2 ppbv of chlorine in the stratosphere, may need some revision when the actual $C\ell_x$ abundance is finally determined.

Scattered sunlight and albedo have only a small effect on our SST results. By not including scattered light or albedo in our model, we slightly underestimate SST ozone changes. Interestingly, the effect of added NO_x on the ozone concentration is largely determined by reaction (4) and thus the NO_2 and O concentration product. Below 30 km the photolysis rates of ozone and NO_2, which control the abundances of O and NO_2, respectively, are strongly dependent on long-wavelength radiation and so they each change by roughly the same fraction due to scattered light (in our simulation, e.g., the ratio of these photo rates is changed by less than 10% at 20 km with and without sunlight scattering). Thus, as the O concentration increases with an increase in scattered light, the NO_2 concentration decreases in a compensating manner.

Actually, the effects of scattered light are more complicated than has just been described. However, its effect on the concentrations of stratospheric trace constituents has been amply discussed in the NASA Chlorofluoromethane Assessment Workshop report (ref. 6). Moreover, in a more detailed study than we have made here, Luther and Wuebbles (ref. 89) have concluded that scattered and reflected sunlight have little effect on calculated SST ozone perturbations.

Diurnal variations (which are approximately simulated in our model — see Turco and Whitten, ref. 20) also affect ozone alteration by SST emissions, but only slightly. In the NASA

Chlorofluoromethane Assessment Workshop report it is pointed out that diurnal variations reduce slightly the effect of NO_x on ozone; we also find this to be true in our calculations. In an earlier study of SST pollution using a time varying model, Chang (ref. 90) obtained a similar result for the effect of seasonal variations on ozone reduction by added nitrogen oxides. While recent calculations show that diurnal variations increase the rate of chlorine-catalyzed ozone destruction by 50% to 70% (e.g., ref. 6), diurnal variations have a much smaller overall effect on predicted ozone perturbations due to NO_x injections – less than 35% according to recent estimates (see table 7).

If we adopt Moortgat's (private communication) formaldehyde quantum yield data for our model, we predict an increase in HO_x of about 15% in the lower stratosphere. As a result, ozone active NO_x is reduced, and Cl_x is increased, although both by smaller amounts (~5% to 10%). Thus, with Moortgat's quantum yield data, a small SST NO_x injection leads to somewhat larger ozone enhancement for 20-km aircraft operation; that is, to an additional 0.3% increase in the stratospheric ozone column for an injection rate of 7×10^8 kg NO_2/yr.

Peroxynitric acid (HO_2NO_2) may be formed by a three-body reaction between HO_2 and NO_2 with a rate constant of 2×10^{-31} cm^6/sec (ref. 66). For a sensitivity test, we have also assumed that HO_2NO_2 is photolyzed into HO_2 and NO_2 at the same rate that H_2O_2 is photolyzed into hydroxyl radicals, and that HO_2NO_2 reacts with OH twice as fast as H_2O_2. Using these rates in our model, the reaction of OH with HO_2NO_2 suppresses the HO_x concentration by 10% to 20% at altitudes below 30 km, but less so at higher altitudes. Moreover, the predicted HO_2NO_2 abundances at all altitudes constitute less than about 10% of the total amount of NO_y, because of its relatively rapid photochemical decomposition in our model. Interestingly, NO and NO_2 concentrations are slightly larger between 15 and 25 km under the conditions of this sensitivity test, because their conversion rate into HNO_3 is slowed somewhat. The SST perturbation results in table 7 show that peroxynitric acid formation leads to half as much ozone production by NO_x as without its formation. However, the absolute effect of HO_2NO_2 on the predicted ozone column change is very small, ~0.2% for an injection rate of 7×10^8 kg NO_2/yr.

Computed SST ozone changes are expected to be quite sensitive to many uncertain photochemical rate coefficients, especially those for the HO_x reactions. In table 7 we show the results of sensitivity tests for two such reactions. The first is reaction (15) between HO_2 and ozone, which is the most important rate limiting reaction in the catalysis of ozone by HO_x in the lower stratosphere. Obviously, from the data in table 7, predicted ozone changes are very sensitive to the rate coefficient for the $HO_2 + O_3$ reaction. To simulate the effect of a change in the HO_x recombination rate (due to processes (21)–(24)), we have increased the rate constant for reaction (24), that is, OH + HNO_3, by a factor of 3. With such a modification, large ozone column depletions due to SST NO_x emission are then computed (see table 7).

To test the sensitivity of ozone perturbations to the ambient water vapor, we have lowered the water vapor mixing ratio at the tropopause from 4 to 2.5 ppmv. (The value 4 ppmv for the water vapor mixing ratio at the tropopause has been suggested by Harries, ref. 91, as an average value based upon many measurements. However, a number of measurements indicate smaller values, near 2.5 ppbv.) Such a change reduces the predicted concentrations of OH, HO_2, HNO_3, and CH_3O_2 in the lower stratosphere (20 km altitude) by about 30, 20, 20, and 35%, respectively. The net effect of lowered HO_x concentrations is an increase in the rate of catalytic destruction of ozone by NO_x and a decrease in the rate of ozone generation by the "smog" reactions (see table 7).

The sensitivity of predicted SST-NO_X ozone column perturbations to HO_X chemistry can be understood in terms of the relative ozone-activity of the HO_X and NO_X catalytic cycles in the lower stratosphere, and the strong interactions between these cycles. In general, as HO_X concentrations are lowered, aircraft NO_X emissions can attack ozone more efficiently. The details of the photochemical processes involved have been discussed in previous sections.

For each of the sensitivity tests listed in table 7, we also give the predicted stratospheric ozone change when water vapor effects are included. The results show quite clearly that the reactions of water vapor deposited by aircraft engines lead, in almost every case, to ozone reductions by SST's flying at 20 km. The basic reason for this effect on ozone is the importance of hydrogen radicals in the ozone budget. Injected water vapor increases HO_X concentrations, even at high altitudes, and increases ozone destruction accordingly (compare the ozone concentration changes with and without H_2O injection shown in fig. 13).

Uncertainties in Model Predictions

In table 8 we have summarized most of the potentially important sources of uncertainty in our SST ozone perturbation estimates as perceived by us during the course of this assessment. We have estimated the magnitudes of the uncertainties associated with many of the aeronomic parameters in our atmospheric model. The derivation of a more quantitative set of uncertainty values would require, first, a statistically meaningful data base for determining individual parameter uncertainty and, second, a detailed model sensitivity analysis. Because the statistical uncertainty of most of the important stratospheric model parameters is unknown, a valid statistical evaluation of total model uncertainty is impossible.

It should be considered that large changes in SST assessments are still conceivable because of the many parameters that are poorly known. Therefore, the assignment of uncertainty or confidence factors does not appear to be useful and, in fact, may be misleading. For example, in the study "Environmental Impact of Stratospheric Flight" by the National Academy of Sciences in 1975 (ref. 2), confidence limits were estimated to be a factor of 2 for flight at 19.5 km and 3 for flight at 16.5 km; in the CIAP report of findings "The Effect of Stratospheric Pollution by Aircraft" by Grobecker, Coroniti and Cannon (ref. 1) the fractional uncertainty (ratio of standard deviation to the mean) in the calculation of fractional ozone change due to SST's was estimated at 0.2. Reference to tables 11 and 12 show that current estimates have changed by factors much larger than the uncertainty factors estimated by the earlier studies; hence those limits were not useful either to scientists or to administrators. There is no reason to believe that the estimation of uncertainty factors for the assessments in this report would be useful either.

5. DISCUSSION

General

Although this SST assessment is not in exact agreement with one presented by the Lawrence Livermore Laboratory group (as reported by Broderick, ref 5), the differences are not very great on an absolute scale. Both show that small column ozone increases might be caused by the NO_X

TABLE 8.– SUMMARY OF UNCERTAINTIES IN PRESENT ESTIMATES OF OZONE PERTURBATIONS BY AIRCRAFT NO_x-H_2O EMISSIONS

Source of uncertainty	Estimated magnitude of the uncertainty $(\pm)^a$ in the stated parameters	Possible effect on ozone perturbations
1. Aircraft NO_x and H_2O emissions: a. Rates, indices b. Meridional spreading c. Traffic density	A factor of $\sim$2	These parameters have a direct effect on ozone reduction estimates.
2. Reaction rate constants, particularly those for: a. $OH + HO_2 \rightarrow H_2O + O_2$	Factor of 2	a. This rate constant affects the OH concentration, and is therefore coupled into the NO_y and $C\ell_x$ reaction cycles which affect ozone.
b. $O_3 + HO_2 \rightarrow OH + O_2$	Factor of 3	b. Same as (a). Also, it determines the rate of odd-oxygen destruction by HO_x in the lower stratosphere. Its importance is reduced by reaction (c).
c. $NO + HO_2 \rightarrow NO_2 + OH$	Factor of 2, although some measurements suggest much smaller values	c. Controls the OH:HO_2 concentration ratio below 35 km; affects the HO_x concentration and the HNO_3:NO_2 ratio (see a and b).
d. $NO + CH_3O_2 \rightarrow NO_2 + CH_3O$	Unknown, but probably a factor of 3	d. "Smog" reaction which creates ozone when NO_2 is photolyzed into O atoms.
e. $HO_2 + NO_2 \xrightarrow{(M)} HO_2NO_2$	Order of magnitude	e. The role of HO_2NO_2 as an NO_y reservoir is not known. HO_2NO_2 may be more important as a hydrogen radical sink if it reacts with OH.
f. $C\ell ONO_2 + H_2O \xrightarrow{aerosol} HNO_3 + HOC\ell$	Order of magnitude	f. Surface hydrolysis may stabilize NO_y as HNO_3 leading to less ozone sensitivity to NO_y.
g. $N_2O + O(^1D) \rightarrow NO + NO$	50%, possibly less	g. and h. These reactions control the ambient NO_y concentration to a large extent, and so the response of ozone to an NO_x injection.
h. $O(^1D) + M \rightarrow O + M$	50%, possibly less	
i. $OH + HNO_3 \rightarrow H_2O + NO_3$	50%, possibly less	i. Same as (a).

^{a}The quoted uncertainty range is meant to roughly encompass the limits of scientifically reasonable values based on the uncertainty and scatter in observational data, but is not meant to preclude values outside this range.

37

TABLE 8.— Continued.

Source of uncertainty	Estimated magnitude of the uncertainty $(\pm)^a$ in the stated parameters	Possible effect on ozone perturbations
3. Photodissociation rates		
a. Solar flux intensity	a. About 10% to 20% above 200 nm, perhaps 30% to 40% below 200 nm, depending on solar activity.	a. Solar fluxes directly affected photodissociation rates. Wavelengths below 200 nm are not important in the stratosphere.
b. Scattered light and albedo	b. Overall about 20% to 30%, but much greater at some wavelengths.	b. Effects on ozone are complex. Basically little difference in computed ozone depletion with and without albedo is found; probably about 10% for $C\ell_x$ ozone perturbations, $\sim$10%–20% for NO_x perturbations.
c. Individual photoprocesses $O_3 + h\nu \rightarrow O(^1D) + O_2$	c. Uncertainty in quantum yield of $O(^1D)$ is about $\pm$30% between 300 and 310 nm, less at shorter wavelengths.	c. The quantum yield of $O(^1D)$ affects $O(^1D)$ concentrations, and thereby, OH and NO_y levels.
$HNO_3 + h\nu \rightarrow OH + NO_2$	Overall cross section uncertainty $\sim$20%	HNO_3 is the most important NO_y reservoir in the stratosphere.
$NO_3 + h\nu \rightarrow NO_2 + O$ $\rightarrow NO + O_2$	Photolysis products unknown; the branching is assumed to be 2/7 NO and 5/7 NO_2.	If the second photolysis channel is active, NO_3 formation is a minor sink for odd-oxygen.
$C\ell ONO_2 + h\nu \rightarrow C\ell O + NO_2$	Overall cross section uncertainty about 20%. In the important long-wavelength absorption tail above 310 nm, it could be larger at stratospheric temperatures.	Chlorine nitrate is a secondary NO_y reservoir. Its production from injected NO_x reduces the effectiveness of $C\ell_x$ catalysis of ozone.
$NO + h\nu \rightarrow N + O$	Estimated photolysis rate uncertainty $\sim$50%	NO photolysis controls the ambient NO_y mixing ratio above 30 km and the incremental NO_y mixing ratio above the injection height.
$CH_2O + h\nu \rightarrow CO + H_2$ $\rightarrow CHO + H$	Factor of 2 in the absolute photolysis rate; in the branching ratio, roughly 50%	The branching ratio controls the rate of production of HO_x from methane oxidation. There are indications that the ratio is pressure dependent.
$H_2O_2 + h\nu \rightarrow OH + OH$	About a factor of 2 in the photolysis rate in the lower atmosphere	H_2O_2 can act as an HO_x recombination sink.

^{a}The quoted uncertainty range is meant to roughly encompass the limits of scientifically reasonable values based on the uncertainty and scatter in observational data, but is not meant to preclude values outside this range.

TABLE 8.– Continued.

Source of uncertainty	Estimated magnitude of the uncertainty $(\pm)^a$ in the stated parameters	Possible effect on ozone perturbations
4. Thermal feedback effect: An ozone change affects stratospheric temperatures which affect rate constants in the ozone chemical cycle. Water vapor injection by SST's also affects the thermal balance of the stratosphere.	Only small temperature perturbations (~5–10 K) are expected. These are hard to determine since heating is not coupled to dynamics in 1-D models.	Negative thermal-chemical feedback effects can lead to smaller net ozone changes. Water vapor addition may cool the stratosphere leading to ozone recovery from water vapor chemical reduction.
5. Diurnal variations	Diurnal variations affect NO_x ozone reduction by about 10% to 20% (compared to about 50% to 70% for Cl_x ozone reductions). Because of the approximate treatment of diurnal variations in our model, there may be a residual uncertainty of ~10%.	Diurnal variations lead to slightly smaller ozone perturbations by NO_x mainly because average daytime NO_2 abundances are slightly reduced.
6. Diffusion coefficients used to simulate vertical "eddy" transport.	A factor of 3 or more in the diffusion coefficient at some altitudes in the lower stratosphere. A factor of ~2 in the resulting residence times in the lower stratosphere.	Changes in stratospheric residence times affect the buildup of injected NO_x and the resultant ozone perturbations. Diffusion also affects ambient NO_y and other species such as O_3 and OH, especially below 30 km where SST perturbations are largest.
7. Ambient H_2O	A factor of 2 in the middle stratosphere, higher in the lower stratosphere, where the variability is also large.	Increased H_2O, for example, leads to more OH and so, more ClO and HNO_3 and less NO_2. Ozone may increase or decrease depending on the relative changes induced in the HO_x, Cl_x, and NO_x catalysis cycles, and in the heat balance of the stratosphere.
8. Ambient OH (whose uncertainty is also related to uncertainties in rate constants and ambient H_2O).	Based on column observations, about a factor of 3 in the stratosphere. No measurements exist in the critical SST region between the troposphere and 30 km.	See (7) for H_2O above; OH controls the important $HNO_3:NO_2$ ratio which has a direct effect on ozone alterations by SST's.

^{a}The quoted uncertainty range is meant to roughly encompass the limits of scientifically reasonable values based on the uncertainty and scatter in observational data, but is not meant to preclude values outside this range.

TABLE 8.– Continued.

Source of uncertainty	Estimated magnitude of the uncertainty (±)[a] in the stated parameters	Possible effect on ozone perturbations
9. Ambient N_2O and NO_y (whose uncertainties are also related to uncertainties in parameters like the rate constant for $N_2O + O(^1D)$, the photolysis rates of N_2O and NO, and the eddy diffusion coefficient).	For N_2O, about ±20%. For total NO_y, about ±40%.	More ambient NO_y can result in smaller perturbations of ozone by injected NO_x, and vice versa; NO_y interacts with the HO_x and $C\ell_x$ chemical cycles, and participates in the "smog" generation of ozone.
10. Ambient NO, NO_2, and HNO_3 (also see items 2, 3, and 9).	For individual species about a factor of 3. For the ratios of species, about the same uncertainty.	The ratios $NO:NO_2$ and $HNO_3:NO_2$ are particularly important for SST calculations as they determine the amount of injected NO_x that actively destroys ozone.
11. Atmospheric chlorine: a. Ambient chlorine concentration b. Chlorine nitrate formation	About a factor of 2 to 3 based on recent $C\ell O$ measurements by Anderson (ref. 50). At least a factor of 2. An upper limit established by Murcray *et al.* (ref. 62) is just barely compatible with present $C\ell ONO_2$ photochemistry.	a and b. The $C\ell_x$ and NO_x ozone catalytic cycles are interactive via the reaction, $NO + C\ell O \rightarrow C\ell + NO_2$, and by $C\ell ONO_2$ formation, which acts as a reservoir for both $C\ell_x$ and NO_x. Increased ambient $C\ell_x$ can result in larger ozone enhancements due to added NO_x because of these interactions.
12. Aerosol interactions: a. $C\ell ONO_2 + H_2O \xrightarrow{\text{aerosol}} HNO_3 + HOC\ell$ b. Direct ozone catalysis c. Stratospheric thermal and dynamic feedback due to aerosol concentration and size changes with SO_x and soot injection. d. Climate effects — feedback on ozone	a. See (2) above. b. Orders of magnitude c. A factor of 3 or 4 d. Unknown	a. See (2) above. b. Ozone destruction on particles is likely to be a negligible ozone sink in the stratosphere. c. Aerosols absorb and scatter radiation, thereby affecting temperature and radiation in the stratosphere. The net effect on ozone is probably small, however. d. As in (c), except that aerosol may have an effect on the troposphere radiation balance with a possible influence on meteorology and stratospheric-tropospheric coupling.

[a]The quoted uncertainty range is meant to roughly encompass the limits of scientifically reasonable values based on the uncertainty and scatter in observational data, but is not meant to preclude values outside this range.

TABLE 8.– Concluded.

Source of uncertainty	Estimated magnitude of the uncertainty $(\pm)^a$ in the stated parameters	Possible effect on ozone perturbations
13. Tropospheric photochemical interactions	Estimated <10% effect on the total ozone column	Ozone behavior in the troposphere is not well established due to the effects of pollutants and meteorology; the modeling of tropospheric ozone is in a preliminary state. The contribution of tropospheric ozone to the total ozone column is less than 10%. Existing estimates of tropospheric ozone perturbations due to SST's show very small effects.
14. Ambient atmospheric temperature and density profiles	Less than 10%, although variability may be significant	In a 1-D model, temperature and density affect reaction rate constants, and O_2 absorption affects photo rates. The use of appropriate standard profiles should be quite acceptable.
15. Natural atmospheric variability	Unknown	The normal variability of species concentrations and air densities and temperatures affect the average rates of chemical kinetic interactions. The effect may be quite large if recently observed fluctuations in OH and CℓO concentrations are reliable indicators of such variability.
16. One-dimensional model limitations a. Absence of horizontal transport	a. Unknown, but probably within a factor of 3	a. Horizontal spreading of injected pollutants directly affects ozone perturbations. Corridor effects can only be roughly estimated with a 1-D model.
b. Species boundary conditions	b. The uncertainty is associated with a lack of information about individual species (see appropriate items above).	b. For the ozone column density change, a model boundary at 10 km has little effect.
c. Vertical grid resolution	c. Probably 10% to 20%	c. A 2-km vertical grid resolution is sufficient for calculating the total ozone column.

^{a}The quoted uncertainty range is meant to roughly encompass the limits of scientifically reasonable values based on the uncertainty and scatter in observational data, but is not meant to preclude values outside this range.
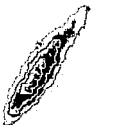
emissions of aircraft flying high in the stratosphere. However, our results also indicate that water emission should be considered in model studies of SST effects on ozone. Taking into account the chemical reactions of emitted H_2O, STT operations could eventually lead to small column ozone reductions. All model predictions currently have large uncertainties associated with them. Because of this, the sign of the change in the stratospheric ozone content when SST's operate at 20 km is in some doubt. Nonetheless, all current indications point toward the likelihood that total ozone column changes caused by SST's would be very small.

In present model calculations of SST effects, ozone production and loss at different altitudes are nearly in balance. Figure 13 shows a typical altitude-dependent ozone perturbation due to SST's flying at 20 km. Clearly, ozone reduction at high altitude is offset by ozone gain at low altitude. The net change in total ozone, which is the difference between the high and low altitude changes, may be very small; for the case shown in figure 13 it is nearly zero. It is therefore understandable that small differences between atmospheric model simulations might be amplified in calculation of the ozone column net change. Based on a comparison between the two 1-D models used in this assessment, we have found that the treatment of methane and water photochemistry and the parameterization of vertical transport are important factors leading to differences in model results. Moreover there are aspects of atmospheric modeling that have not yet been adequately explored, such as radiative-dynamical feedback effects and aerosol interactions. Further improvements in model predictions can also be expected as the chemistry of the lower stratosphere is better defined through continuing atmospheric observations and laboratory measurements.

Assessments

The information in this report can be used to make SST-ozone assessments for a range of fleet sizes, engine emission indexes, and flight altitudes. (Assessments based on the data in this report should be restricted to the range of NO_x emissions given in fig. 1, because ozone perturbations are not additive for larger injections of NO_x.) Figure 1 allows the conversion of SST fleet size into an NO_x emission rate (the total amount of NO_x in the form of NO_2 emitted per year) for engines representative of near-term technology or far-term technology. The figure is based on the fuel flow rates, emission indexes, and flight durations given in section 2; although these values are reasonable current estimates, any other values can be incorporated through equation (1). For the SST-NO_x injection rate determined from figure 1, the curves in figure 15 (an expanded version of parts of figs. 11(a) and (b)) can be used to calculate the ozone change caused by those aircraft if they fly at 20 km. (Figure 15 is an enlargement of part of fig. 11, and is included in this section for convenience.) If assessments at other flight altitudes are desired, figure 12 can be used to derive, roughly, the ratio of the depletion caused by flights at 20 km to the depletion caused by flights at any other altitude. (This procedure is exact for an injection rate of 7×10^8 kg NO_2/yr but

Figure 15.— Expanded portion of figure 11.

42

becomes progressively worse for injection rates different from this value, particularly for larger injections.)

The procedure is reversed to determine the number of aircraft that can operate without exceeding a specified depletion limit. The amount of NO_x that will produce the specified depletion for operations at 20 km are found from figure 15. Figure 1 then provides the number of aircraft that will emit that amount of NO_x. Again, the ratio in figure 12 can be used to determine, roughly, the number of aircraft at any other altitude that will produce approximately the same effect.

Table 9 summarizes the assessment for 100 Type-A aircraft. Table 10 summarizes the assessment for Type-B aircraft. The specific characteristics of type-A and type-B aircraft are presented in table 1 (section 2). The principal difference between the two aircraft (with respect to this assessment), is their flight altitude; Type A flies at 20 km, Type B at 17.5 km. Because there is no clear-cut way to select a vertical eddy diffusion profile we give results for the Dickinson-Chang (DC) profile and the Wofsy-type (WT) profile. Assessments with the DC profile show less ozone depletion because, with that profile, NO_x (and H_2O) is removed more quickly from the lower stratosphere.

TABLE 9.– ESTIMATE OF THE STRATOSPHERIC OZONE COLUMN CHANGE DUE TO 100 TYPE A AIRCRAFT[a] (CRUISE ALTITUDE 20 KM[b])

Engine technology	NO_x emission index, g NO_2/kg fuel	NO_x emission, 10^8 kg NO_2/yr	H_2O emission, 10^{10} kg H_2O/yr	Percent ozone change			
				NO_x and H_2O		NO_x only	
				DC	WT	DC	WT
Near term	15.6	1.47	1.25	0.07	0.03	0.12	0.12
Far term — high	6	.57	1.25	.0	−.06	.05	.05
Far term — low	2	.19	1.25	−.03	−.08	.02	.02

[a]Because these reductions are so small and were calculated using interpolated curves for small injection rates, there is considerable numerical uncertainty in their values. Hence ozone changes are rounded to the nearest hundredth percent.

[b]See table 1 and section 2 for other flight characteristics.

TABLE 10.– ESTIMATE OF THE STRATOSPHERIC OZONE COLUMN CHANGE DUE TO 100 TYPE B AIRCRAFT[a] (CRUISE ALTITUDE 17.5 KM[b])

Engine technology	NO_x emission index, g NO_2/kg fuel	NO_x emission, 10^8 kg NO_2/yr	H_2O emission, 10^{10} kg H_2O/yr	Percent ozone change			
				NO_x and H_2O		NO_x only	
				DC	WT	DC	WT
Near term	18	1.65	1.17	0.10	0.06	0.13	0.13
Far term — high	7	.64	1.17	.02	−.02	.05	.05
Far term — low	3	.27	1.17	−.01	−.05	.02	.02

[a]Because these reductions are so small and were calculated using interpolated curves for small injection rates, there is considerable numerical uncertainty in their values. Hence, ozone changes are rounded to the nearest hundredth percent.

[b]See table 1 and section 2 for other flight characteristics.

The basic groundwork for making aircraft assessments was developed by the DOT during the CIAP activity. Both CIAP and the NAS have published aircraft assessments in the past (referenced in section 1). Although atmospheric models have been refined in many respects since those assessments were reported (e.g., diurnal averaging, radiation scattering, inclusion of chlorine chemistry, etc.), the most important changes have resulted from the new $HO_2 + NO$ reaction rate measurement. A comparison of model predictions obtained using the DC and WT vertical transport parameterizations (fig. 11) also emphasizes the importance of lower stratospheric dynamics in SST assessments.

To illustrate the changes in SST calculations caused by recent developments in stratospheric aeronomy, we have compared the earlier CIAP and NAS assessments with the present one in tables 11 and 12 (for the same aircraft exhaust injection rates and flight altitudes).

TABLE 11.– COMPARISON OF THE PRESENT OZONE PERTURBATION ESTIMATES WITH THE NAS ASSESSMENTS[a]

Aircraft	NO_X emission rate, 10^8 kg NO_2/yr	Percent ozone column change (global average)				
		NAS assessment	This report (near-term technology)			
			NO_X and H_2O emissions		NO_X emissions only	
			DC	WT	DC	WT
Present SST[b]	0.63	-0.72	0.03	0.01	0.04	0.05
Large SST[c]	1.64	-3.27	0.07	0.03	0.13	0.13

[a]Because these reductions are so small and were calculated using interpolated curves for small injection rates, there is considerable numerical uncertainty in their values. Hence ozone changes are rounded to the nearest hundredth percent.

[b]Cruise altitude 16.5 km.

[c]Cruise altitude 19.5 km.

TABLE 12.– COMPARISON OF THE PRESENT OZONE PERTURBATION ESTIMATES WITH THE CIAP ASSESSMENTS[a]

Aircraft	NO_X emission rate, 10^8 kg NO_2/yr	Percent ozone column change (global average)				
		CIAP assessment	This report (near-term technology)			
			NO_X and H_2O emissions		NO_X emissions only	
			DC	WT	DC	WT
Present SST[b]	0.54	-0.39	0.02	0.0	0.04	0.04
Large SST[c]	1.08	-1.74	0.04	0.02	0.09	0.09

[a]Because these reductions are so small and were calculated using interpolated curves for small injection rates, there is considerable numerical uncertainty in their values. Hence ozone changes are rounded to the nearest hundredth percent.

[b]Cruise altitude 16.5 km.

[c]Cruise altitude 19.5 km.

CONCLUDING REMARKS

It is clear from the above discussion that supersonic transport assessments have changed significantly since the CIAP. Figure 16, which is an adaptation of figure 3 in Broderick (ref. 5), summarizes the effect of a series of model revisions on the aircraft assessment reported here. It shows the evolution during the course of this assessment of our calculated SST ozone perturbations for an equivalent NO_x injection rate of 3.5×10^8 kg NO_2/yr at 20 km. The initial model utilized the January 1977 recommended NASA-CFM Workshop chemical kinetic data and included water vapor injection at the rate of $550 H_2O$ molecules per NO_x molecule (which corresponds to an NO_x engine emission index of 6 g NO_2/kg fuel). "$NO + HO_2$" indicates the adoption of the new (larger) rate constant $(8 \times 10^{-12}$ cm^3/sec) for reaction (2); "$J_{H_2O_2}$" shows the effect of including H_2O_2 absorption above 255 nm; "CH_4" illustrates the effect of using a rate constant of 2×10^{-12} cm^3/sec for the reaction of NO with CH_3O_2; and "no H_2O" gives the result when exhaust water vapor is not injected along with NO_x.
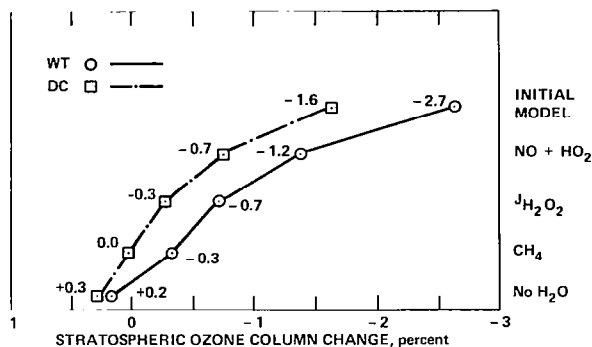

Figure 16.— Evolution during the course of this assessment of our calculated ozone perturbations.

Uncertainties in aeronomic models are such that SST-ozone perturbation estimates can range from small ozone column increases to small column decreases due to aircraft exhaust; the principal sources of the differences in model predictions appear to be in the treatment of hydrogen radical chemistry in the lower stratosphere and water vapor emissions by aircraft engines. In any case, it appears that the effect of commercial high-altitude aviation on the total content of ozone in the stratosphere should be negligible for the next quarter century. However, it must be emphasized that this evaluation is subject to change as our knowledge of the stratosphere expands. In order to increase confidence in SST assessments, therefore, additional studies of the lower stratosphere must be initiated, and those in progress, continued.

Ames Research Center
    National Aeronautics and Space Administration
        Moffett Field, California 94035, April 3, 1978

APPENDIX A

ENGINE CRUISE EMISSION ESTIMATES

Gregory M. Reck
Lewis Research Center

APPROACH

Cruise NO_X emission estimates were made for three types of aircraft: wide-body subsonic, supersonic, and a baseline supersonic. The baseline supersonic aircraft was chosen to be the Langley Mach 2.7 arrow-wing configuration designated the AST-100 (ref. 14). For each aircraft type, estimates were made for several levels of engine technology representing current, near-term and far-term engines. The near-term estimates represent the implementation of technology in production engines in the early or mid-1980s, while technology inherent in the far-term estimates will not appear in production before the 1990s.

Only limited emissions data have been acquired from aircraft turbine engines operating at altitude cruise conditions (typically, during altitude wind-tunnel tests). The bulk of the available emissions data has been acquired during sea-level static tests or from combustor component tests. These data must then be adjusted or extrapolated to obtain estimates of emissions at cruise conditions. A number of expressions have been developed for adjusting emissions data to different combustor operating conditions. These expressions typically employ correlations of NO_X emissions with inlet temperature, inlet pressure, equivalence ratio or outlet temperature, and other factors. These expressions are reliable when applied to the same type of combustor from which the correlations were developed and within the range of conditions over which the correlations were derived.

The following expression was used in developing the NO_X emissions estimates contained herein which required an adjustment of conditions:

$$(EI)_2 = (EI)_1 \left[\frac{(P_3)_2}{(P_3)_1}\right]^{0.5} \exp\left[\frac{(T_3)_2 - (T_3)_1}{288}\right]\left[\frac{(T_4)_2}{(T_4)_1}\right] \tag{A1}$$

where

EI emission index, g NO_2/kg fuel burned

P_3 combustor inlet pressure, atm

T_3 combustor inlet temperature, K

T_4 combustor exit temperature, K

46

Subscripts:

1   initial condition

2   final condition

The correlation was derived from emissions data acquired from conventional diffusion flame combustors. As a result, its accuracy is uncertain when applied to different combustor types, such as lean premixed-prevaporized. However, limited data from flame-tube tests have supported the correlation.

A serious limitation regarding the correlation is the deficiency of emissions data at high pressures and temperatures. The trend in advanced technology engines toward higher cycle pressure ratios for improved efficiency results in more severe combustor conditions from NO_x emissions point of view. It can be seen from equation (A1) that NO_x increases in proportion to the square root of pressure and exponentially with increases in inlet temperature. Continuing experimental activities are directed toward extending the data base used in developing correlating expressions.

SUBSONIC AIRCRAFT CRUISE NO_x EMISSIONS

The cruise NO_x emissions estimates for subsonic aircraft are shown in table 13. The emissions values shown for current subsonic aircraft are taken from references 92 and 93, and represent emissions from production combustors of the engines powering wide-body commercial transport aircraft.

The NO_x emission estimate for near-term emission technology is derived from the NASA Experimental Clean Combustor Program (ECCP). The goal of the ECCP is to develop and demonstrate combustor technology to significantly lower pollutant emission levels from current engine combustors. The emissions goals established for the program are directed toward low-altitude (idle, taxi, takeoff, landing) operations, although emissions reductions have been achieved at intermediate power settings. The ECCP has been conducted in three phases. Phases I and II consisted of experimental screening and development of promising concepts. Phase III, which is currently in progress, consists of an engine demonstration of the selected concepts. The emission level shown in table 13 was taken from Phase II results and represents data acquired from advanced combustors run at simulated cruise conditions. The NO_x emissions estimate shown for far-term technology is derived from the NASA Stratospheric Cruise Emission Reduction Program (SCERP). The SCERP objective is to develop and demonstrate the technology necessary to reduce cruise NO_x emissions by a factor of 6 from current levels. Lean premixed-prevaporized combustion is being examined in SCERP as an approach to achieving the program goal of an emission index of 3 g NO_2/kg fuel. The lower value of 1 g NO_2/kg fuel also shown in table 14 is a very optimistic projection based on

TABLE 13.— SUBSONIC AIRCRAFT CRUISE EMISSION ESTIMATES: M = 0.85, ALTITUDE = 10.7 km

Level of combustor technology	Engine	NO_x emissions index, g NO_2/kg fuel
Current	CF6-50 JT9D-7	16 22
Near-term	---	8
Far-term	---	1 − 3

47

TABLE 14.– BASELINE SUPERSONIC CRUISE AIRCRAFT CRUISE EMISSION
ESTIMATES: M = 2.7, ALTITUDE = 20 km

Level of combustor technology	Initial conditions				Baseline supersonic aircraft engine conditions			Emission estimate
	T_{in}, K	P_{in}, atm	T_{out}, K	EI_{NO_x}, g/kg	T_{in}, K	P_{in}, atm	T_{out}, K	EI_{NO_x}, g/kg
Near-term	733	11.4	1449	8.0	942	7.4	1700	15.6
Far-term	733	10.0	1449	1-3	942	7.4	1700	2-6

limited experimental data from premixing-prevaporizing flame-tube combustors which have been optimized for fixed conditions.

The SCERP goal is associated with far-term technology because the lean-burn approach represents a higher development risk than the staged combustor approach developed in the ECCP. The application of the lean-burn technique will likely require technology not found in current engines such as variable combustor geometry and digital fuel controls. The initial phase of SCERP consists of a number of fundamental studies directed toward establishing a design data base. This data base will then be used to access the feasibility of proposed concepts before deciding whether or not to proceed with experimental concept testing. Subsequently, SCERP would proceed through combustor screening, development, and eventual demonstration in a candidate engine in the early 1980s.

BASELINE SUPERSONIC AIRCRAFT CRUISE NO_x EMISSIONS

The AST-100 baseline supersonic aircraft emissions estimates are shown in table 14. The table includes the initial data or information from which the estimate was made under "Initial Conditions." Equation (A1) was used to extrapolate the initial information to the engine operating conditions. The engine conditions shown in the table were derived from an engine performance computer routine for a single-spool turbojet with variable turbine geometry and no augmentation. ECCP technology was used for the near-term estimate and SCERP technology was employed for the far-term estimate.

The initial conditions for both the near-term and the far-term cases are representative of subsonic aircraft engines. The inlet pressure for the supersonic engines is lower than for the subsonic engines; however, both the inlet and outlet temperatures are higher. Since the correlating expression is much more sensitive to temperature, the extrapolated emission levels are nearly twice the emissions of the subsonics.

SUPERSONIC CRUISE AIRCRAFT NO$_X$ EMISSIONS

The NO$_X$ emission estimates for the various levels of supersonic aircraft engine technology are presented in table 15. The estimates shown are for the cruise design point conditions listed and do not take into consideration variations in altitude and engine conditions which may occur along the flight path. Cruise climb flight trajectories typically flown by supersonic aircraft do involve altitude changes.

The emission estimate for the Olympus 593 is taken from reference 94. This afterburning engine represents current technology and is being flown on the Concorde. The engine emissions level is approximately the same as current subsonic engines. The cycle pressure ratio is lower than the subsonics; however, the supersonic ram recovery results in a higher combustor inlet temperature.

The near-term technology emissions estimate is based on ECCP combustor emissions data. These data were extrapolated to the combustor conditions of the Pratt & Whitney VSCE 502B, an advanced supersonic propulsion study engine. This engine is a duct-burning variable cycle engine with a core cycle pressure ratio substantially higher than for current supersonic aircraft engines. The high core pressures and temperatures result in an emissions estimate which is a factor of 4 larger than the initial ECCP Phase II data; however, the accuracy of the extrapolation is uncertain over such an extreme range of conditions. Since the VSCE 502B is a study engine, the combustor conditions cited are subject to change. These conditions represent an optimum cycle for a specific aircraft operating within given constraints. Any change in the airframe or the flight constraints would likely result in a change in combustor conditions.

The near-term estimate for the duct burner emissions is based on an analytical study of low emissions, high performance duct burners reported in reference 95. This estimate is based on a variation of a combustor concept developed for the ECCP. The duct burner conditions are significantly less severe than the core conditions resulting in a much lower level of emissions.

TABLE 15.— SUPERSONIC AIRCRAFT CRUISE EMISSION ESTIMATES

Level of combustor technology		Initial conditions				Supersonic aircraft engine conditions			Emission estimates	
		T_{in}, K	P_{in}, atm	T_{out}, K	EI_{NO_X}, g/kg	T_{in}, K	P_{in}, atm	T_{out}, K	Component EI_{NO_X}, g/kg	Engine EI_{NO_X}, g/kg
Current (Olympus 593)[a]						824	6.5	1320	---	18
Near-term[b]	Core	733	10.0	1449	8	983	14.2	1756	30	18
	Duct					604	2.5	1000	2.75	
Far-term	Core	733	10.0	1449	1-3	983	14.2	1756	3-10	3-7
	Duct					604	2.5	1000	2.75	

[a] Cruise at Mach 2.0 and 17.7 km.

[b] Cruise at Mach 2.32 and 17.5 km.

When the emissions contribution of the core combustor and the duct burner are combined, the resulting engine emission level is approximately an average of the two. Although more airflow passes through the duct burner (the variable cycle bypass ratio is approximately 1.5 at supersonic cruise), which has a lower component emission index than the core, the core fuel-air ratio is higher resulting in nearly equal emissions contributions by each. The advanced technology engine emissions level is essentially the same as for current turbojet technology. The improved emissions characteristics of the ECCP technology is offset by the effects of the higher cycle pressure ratio.

The far-term emissions estimate shown in table 15 is also calculated for the VSCE 502B variable cycle engine; however, the core emissions level was based on the emissions goal of SCERP. The duct burner emissions level is the same as that used in the near-term estimate since further improvement in emissions may be difficult. It is apparent that far-term technology is required before significant reductions below current emissions levels can be achieved for supersonic aircraft engines.

CRUISE FUEL CONSUMPTION ESTIMATES

Table 16 lists the fuel consumption estimates for the various aircraft types and levels of combustor technology. The estimates for the subsonic aircraft were derived from the cruise design point conditions given in references 92 and 93. The baseline supersonic aircraft fuel consumption was derived from a computer routine for a single-spool turbojet. The Olympus 593 fuel consumption was taken from reference 4 (monograph 2). The fuel consumption for the VSCE 502B was derived from information contained in references 94 and 95.

TABLE 16.– CRUISE FUEL CONSUMPTION ESTIMATES

Aircraft type	Level of combustor technology	Engine	Aircraft	Mach no.	Altitude, km	Number of engines	Fuel consumption per aircraft, kg/hr
Subsonic	Current near-term	JT9D-7	B747	0.85	10.7	4	12,720
	far-term	CF6-50	DC10	0.85	10.7	3	9,480
Baseline supersonic	Near-term far-term	---	AST-100	2.7	20	4	44,100[a]
Supersonic	Current	Olympus 593	Concorde	2.0	17.7	4	16,800
	Near-term Far-term	VSCE-502B	---	2.32	17.5	4	41,050[a]

[a]Initial fuel consumption rate.

REFERENCES

1. Grobecker, A. J.; Coroniti, S. C.; and Cannon, R. H.: Report of Findings: The Effects of Stratospheric Pollution by Aircraft. U.S. Department of Transportation Report DOT-TSC-75-50, Dec. 1974.

2. Environmental Impact of Stratospheric Flight: Biological and Climatic Effects of Aircraft Emissions in the Stratosphere. National Academy of Sciences, Washington, 1975.

3. Halocarbons: Environmental Effects of Chlorofluoromethane Release, National Academy of Sciences, Washington, 1976.

4. CIAP: Climate Impact Assessment Program Monographs. A. J. Grobecker and S. C. Coroniti, eds., U.S. Department of Transportation Reports DOT-TSC-51 to 56, September 1975.

5. Broderick, A. J.: Stratospheric Effects from Aviation. AIAA paper 77-799, presented at AIAA/SAE 13th Propulsion Conference, Orlando, Florida, July 11–13, 1977.

6. Hudson, R. D., ed.: Chlorofluoromethanes and the Stratosphere. NASA Reference Publication 1010, Nat. Tech. Info. Serv., Springfield, Virginia, Aug. 1977.

7. Turco, R. P.; and Whitten, R. C.: The NASA Ames Research Center One- and Two-Dimensional Stratospheric Models. Part I: The One-Dimensional Model. NASA TP-1002, 1977.

8. Whitten, R. C.; Borucki, W. J.; Watson, V. R.; Shimazaki, T.; Woodward, H. T.; Riegel, C. A.; Capone, L. A.; and Becker, T.: The NASA Ames Research Center One- and Two-Dimensional Stratospheric Models. Part II. The Two-Dimensional Model, NASA Technical Paper 1003, 1977.

9. Widhopf, George F.; Glatt, Leslie; and Kramer, Raymond F.: Potential Ozone Column Increase Resulting from Subsonic and Supersonic Aircraft NO_x Emissions. AIAA Journal, vol. 15, no. 9, 1977, pp. 1322–1330.

10. Howard, Carleton J.; and Evenson, K. M.: Kinetics of the Reaction of HO_2 with NO. Geophys. Res. Lett., vol. 4, no. 10, 1977, pp. 437–440.

11. Borucki, W. J.; Whitten, R. C.; Watson, V. R.; Woodward, H. T.; Riegel, C. A.; Capone, L. A.; and Becker, T.: Model Predictions of Latitude-Dependent Ozone Depletion Due to Supersonic Transport Operations. AIAA Journal, vol. 14, no. 12, 1976, pp. 1738–1745.

12. Hidalgo, H.; and Crutzen, P. J.: The Tropospheric and Stratospheric Composition Perturbed by NO_x Emissions of High Altitude Aircraft. J. Geophys. Res., vol. 82, no. 37, 1977, pp. 5833–5886.

13. Tuck, A. F.: Numerical Model Studies of the Effect of Injected Nitrogen Oxides on Stratospheric Ozone. Proc. Roy. Soc. London A, vol. 355, no. 168, 1977, pp. 267–299.

14. Baber, H. T.; and Swanson, E. E.: Advanced Supersonic Technology Concept AST-100 Characteristics Developed in a Baseline-Update Study. NASA TM X-72,815, 1976.

15. Oliver, R. C.; Bauer, E.; Hidalgo, H.; Gardner, K. A.; and Wasylkiwskyj, W.: Aircraft Emissions: Potential Effects on Ozone and Climate. A Review Final Progress Report, U.S. Department of Transportation Report FAA-EQ-77-3, March 1977.

16. Whitten, R. C.; and Turco, R. P.: Perturbations of the Stratosphere and Mesosphere by Aerospace Vehicles. AIAA Journal, vol. 12, no. 8, 1974, pp. 1110–1117.

17. Whitten, R. C.; Borucki, W. J.; and Turco, R. P.: Possible Ozone Depletions Following Nuclear Explosions. Nature, vol. 257, no. 5521, 1975, pp. 38–39.

18. Whitten, R. C.; Borucki, W. J.; Poppoff, I. G.; and Turco, R. P.: Preliminary Assessment of the Potential Impact of Solid-Fueled Rocket Engines in the Stratosphere. J. Atmos. Sci., vol. 32, no. 3, 1975, pp. 613–619.

19. Turco, R. P.; and Whitten, R. C.: Chlorofluoromethanes in the Stratosphere and Some Possible Consequences for Ozone. Atmos. Env., vol. 9, no. 12, 1975, pp. 1045–1061.

20. Turco, R. P.; and Whitten, R. C.: A Note on the Diurnal Averaging of Aeronomical Models. J. Atmos. Terr. Phys., vol. 40, no. 1, 1978, pp. 13–20.

21. U.S. Standard Atmosphere, U.S. Government Printing Office, Washington, 1976.

22. Duewer, William H.; Wuebbles, Donald J.; Ellsaesser, Hugh W.; and Chang, Julius S.: NO_x Catalytic Ozone Destruction: Sensitivity to Rate Coefficients. J. Geophys. Res., vol. 82, no. 6, 1977, pp. 935-942.

23. Luther, F. M.; and Duewer, W. H.: Effect of Changes in Stratospheric Water Vapor and Abundance on Predicted Ozone Reductions. IAGA/IAMAP Joint Assembly, Seattle, Washington, August 22–September 3, 1977.

24. Luther, Frederick M.; Wuebbles, Donald J.; and Chang, Julius S.: Temperature Feedback in a Stratospheric Model. J. Geophys. Res., vol. 82, no. 81, 1977, pp. 4935–4942.

25. Wofsy, Steven C.; and McElroy, Michael B.: On Vertical Mixing in the Upper Stratosphere and Lower Mesosphere. J. Geophys. Res., vol. 78, no. 15, 1973, pp. 2619-2624.

26. Johnston, Harold S.; Kattenhorn, David; and Whitten, Gary: Use of Excess Carbon 14 Data to Calibrate Models of Stratospheric Ozone Depletion by Supersonic Transports. J. Geophys. Res., vol. 81, no. 3, 1976, pp. 368–380.

27. Hunten, D. M.: Residence Times of Aerosols and Gases in the Stratosphere. Geophys. Res. Lett., vol. 2, no. 1, 1975, pp. 26–28.

28. Bauer, E.; Oliver, R. C.; and Wasylkiwskyj, W.: On the Use of Zr-95 Data from Chinese Atmospheric Thermonuclear Explosions to Study Stratospheric Transport in a One-Dimensional Parameterization. J. Geophys. Res., in press, 1978.

29. Mason, Allen S.; and Ostlund, H. Göte: Atmospheric HT and HTO 3. Vertical Transport of Water in the Stratosphere. J. Geophys. Res., vol. 81, no. 30, 1976, pp. 5349-5352.

30. Schmeltekopf, A. L.; Albritton, D. L.; Crutzen, P. J.; Goldan, P. D.; Harrup, W. J.; Henderson, W. R.; McAfee, J. R.; McFarland, M.; Schiff, H. I.; Thompson, T. L.; Hofmann, D. J.; and Kjome, N. T.: Stratospheric Nitrous Oxide Altitude Profiles at Various Latitudes. J. Atmos. Sci., vol. 34, no. 5, 1977, pp. 729–736.

31. Ackerman, M.; Frimout, D.; and Muller, C.: Stratospheric CH_4, HCℓ, and CℓO and the Chlorine-Ozone Cycle. Nature, vol. 269, no. 5625, 1977, pp. 226–227.

32. Ehhalt, D. H.; Heidt, L. E.; and Martell, E. A.: The Concentration of Atmospheric Methane Between 44 and 62 km Altitude. J. Geophys. Res., vol. 77, no. 12, 1972, pp. 2193–2196.

33. Ehhalt, D. H.; and Heidt, L. E.: Vertical profiles of CH_4 in the Troposphere and Stratosphere. J. Geophys. Res., vol. 78, no. 29, 1973, pp. 5265–5271.

34. Ehhalt, D. H.: Sampling of Stratospheric Trace Constituents. Canad. J. Chem., vol. 52, no. 8, 1974, pp. 1510–1518.

35. Martell, E. A.; and Heidt, L. E.: Hydrogen and Carbon Compounds in the Upper Stratosphere and Lower Mesosphere. Proceedings of the International Conference on Structure, Composition, and General Circulation of the Upper and Lower Atmospheres and Possible Anthropogenic Perturbations, IAMAP, Melbourne, Australia, Jan. 11–25, 1974, pp. 223–229.

36. Ehhalt, D. H.; Heidt, L. E.; Lueb, R. H.; and Roper, N.: Vertical Profiles of CH_4, H_2, CO, N_2O, and CO_2 in the Stratosphere. Proceedings of the Third Conference on the Climatic Impact Assessment Program, February 26–March 1, 1974; A. J. Broderick and T. M. Hard, eds., U.S. Department of Transportation Report DOT-TSC-OST-74-15, Nov. 1974, pp. 153–160.

37. Vedder, J. F.; Tyson, B. J.; Brewer, R. B.; Boitnott, C. A.; and Inn, E. C. Y.: Lower Stratosphere Measurements of Variation with Latitude of $CF_2C\ell_2$, $CFC\ell_3$, $CC\ell_4$, and N_2O Profiles in the Northern Hemisphere. Geophys. Res. Lett., vol. 5, no. 1, 1978, pp. 33–36.

38. Williams, Walter J.; Kosters, John J.; Goldman, Aaron; and Murcray, David G.: Measurements of Stratospheric Halocarbon Distributions Using Infrared Techniques. Geophys. Res. Lett., vol. 3, no. 7, 1976, pp. 379–382.

39. Heidt, L. E.; Lueb, R.; Pollock, W.; and Ehhalt, D. H.: Stratospheric Profiles of $CC\ell_3F$ and $CC\ell_2F_2$. Geophys. Res. Lett., vol. 2, no. 10, 1975, pp. 445–447.

40. Schmeltekopf, A. L.; Goldan, P. D.; Henderson, W. R.; Harrop, W. J.; Thompson, T. L.; Fehsenfeld, F. C.; Schiff, H. I.; Crutzen, P. J.; Isaksen, I. S. A.; and Ferguson, E. E.: Measurements of Stratospheric $CFC\ell_3$, $CF_2C\ell_2$, and N_2O. Geophys. Res. Lett., vol. 2, no. 9, 1975, pp. 393–396.

41. Krueger, Arlin J.; and Minzner, Raymond A.: A Mid-Latitude Ozone Model for the 1976 U.S. Standard Atmosphere. J. Geophys. Res., vol. 81, no. 24, 1976, pp. 4447–4481.

42. Loewenstein, M.; Savage, H. F.; and Whitten, R. C.: Seasonal Variations of NO and O_3 at Altitudes of 18.3 and 21.3 km. J. Atmos. Sci., vol. 32, no. 11, 1975, pp. 2185–2190.

43. Ridley, B. A.; Schiff, H. I.; Shaw, A.; and Megill, L. R.: In-situ Measurements of NO in the Stratosphere Using Chemiluminescence. Proceedings of the Third Conference on the Climatic Impact Assessment Program, February 26–March 1, 1974; A. J. Broderick and T. M. Hard, eds.; U.S. Department of Transportation Report DOT-TSC-OST-74-15, Nov. 1974, p. 193.

44. Patel, C. K. N.; Burkhardt, E. G.; and Lambert, C. A.: Spectroscopic Measurements of Stratospheric Nitric Oxide and Water Vapor. Science, vol. 184, no. 4142, 1974, pp. 1173–1176.

45. Ackerman, M.; Fontanella, J. C.; Frimout, D.; Girard, A.; Louisnard, N.; and Muller, C.: Simultaneous Measurements of NO and NO_2 in the Stratosphere. Planet. Space Sci., vol. 23, no. 9, 1975, pp. 651–660.

46. Murcray, D. G.; Goldman, A.; Williams, W. J.; Murcray, F. H.; Brooks, J. N.; Van Allen, J.; Stocker, R. N.; Kosters, J. J.; Barker, D. B.; and Snider, D. E.: Recent Results of Stratospheric Trace-Gas Measurements from Balloon-Borne Spectrometers. Proceedings of the Third Conference on the Climate Impact Assessment Program, February 26–March 1, 1974, A. J. Broderick and T. M. Hard, eds., U.S. Department of Transportation Report DOT-TSC-OST-74-15, Nov. 1974, pp. 184–192.

47. Ackerman, M.; and Muller, C.: Stratospheric Nitrogen Dioxide from Infrared Absorption Spectra. Nature, vol. 240, no. 5379, 1972, pp. 300–301.

48. Anderson, James G.: Rocket Measurement of OH in the Mesosphere. J. Geophys. Res., vol. 76, no. 31, 1971, pp. 7820–7824.

49. Wang, Charles C.; Davis, L. I.; Wu, C. H.; Japar, S.; Niki, H.; and Weinstock, B.: Hydroxyl Radical Concentrations Measured in Ambient Air. Science, vol. 189, no. 4205, pp. 797–800.

50. Anderson, J. G.: The Absolute Concentration of OH($X^2\Pi$) in the Earth's Stratosphere. Geophys. Res. Lett., vol. 3, no. 3, 1976, pp. 165–168.

51. Burnett, Clyde R.: Terrestrial OH Abundance Measurements by Spectroscopic Observation of Resonance Absorption of Sunlight. Geophys. Res. Lett., vol. 3, no. 6, 1976, pp. 319–322.

52. Davis, D. D.; Heaps, W.; and McGee, T.: Direct Measurements of Natural Tropospheric Levels of OH via an Aircraft Borne Tunable Dye Laser. Geophys. Res. Lett., vol. 3, no. 6, 1976, pp. 331–333.

53. Perner, D.; Ehhalt, D. H.; Pätz, H. W.; Platt, U.; Röth, E. P.; and Volz, A.: OH Radicals in the Lower Troposphere. Geophys. Res. Lett., vol. 3, no. 8, 1976, pp. 466–468.

54. Lazrus, A. L.; Gandrud, B. W.; Woodard, R. N.; and Sedlacek, W. A.: Stratospheric Halogen Measurements. Geophys. Res. Lett., vol. 2, no. 10, 1975, pp. 439–441.

55. Lazrus, A. L.; Gandrud, B. W.; Woodard, R. N.; and Sedlacek, W. A.: Direct Measurements of Stratospheric Chlorine and Bromine. J. Geophys. Res., vol. 81, no. 6, 1976, pp. 1067–1070.

56. Lazrus, A. L.; Gandrud, B. W.; Greenberg, J.; Bonelli, J.; Mrox, E.; and Sedlacek, W. A.: Midlatitude Seasonal Measurements of Stratospheric Acidic Chlorine Vapor. Geophys. Res. Lett., vol. 4, no. 12, 1977, pp. 587–589.

57. Farmer, C. B.; Raper, O. F.; and Norton, R. H.: Spectroscopic Detection and Vertical Distribution of HCℓ in the Troposphere and Stratosphere. Geophys. Res. Lett., vol. 3, no. 1, 1976, pp. 13–16.

58. Williams, W. J.; Kosters, J. J.; Goldman, A.; and Murcray, D. G.: Measurement of the Stratospheric Mixing Ratio of HCℓ Using Infrared Absorption Technique. Geophys. Res. Lett., vol. 3, no. 7, 1976, pp. 383–385.

59. Ackerman, M.; Frimout, D.; Girard, A.; Gottignies, M.; and Muller, C.: Stratospheric HCℓ from Infrared Spectra. Geophys. Res. Lett., vol. 3, no. 2, 1976, pp. 81–83.

60. Eyre, J. R.; and Roscoe, H. K.: Radiometric Measurement of Stratospheric HCℓ, Nature, vol. 266, no. 5599, 1977, pp. 243–244.

61. Raper, O. F.; Farmer, C. B.; Toth, R. A.; and Robbins, B. D.: The Vertical Distribution of HCℓ in the Stratosphere. Geophys. Res. Lett., vol. 4, no. 11, 1977, pp. 531–534.

62. Murcray, D. G.; Goldman, A.; Williams, W. J.; Murcray, F. H.; Bonomo, F. S.; Bradford, C. M.; Cook, G. R.; Hanst, P. L.; and Molina, M. J.: Upper Limit for Stratospheric CℓONO$_2$ from Balloon-Borne Infrared Measurements. Geophys. Res. Lett., vol. 4, no. 6, 1977, pp. 227–230.

63. Vlasov, M. N.: The Photochemistry of Excited Species. J. Atmos. Terr. Phys., vol. 38, no. 8, pp. 807–820.

64. Cox, R. A.: Current Status of Some Kinetics Data Required for Modeling Tropospheric Photochemistry. IAGA/IAMAP Joint Assembly, Seattle, Washington, August 22 to September 3, 1977.

65. Turco, R. P.: Photodissociation Rates in the Atmosphere Below 100 km. Geophys. Surveys, vol. 2, no. 2, 1975, pp. 153–192.

66. Howard, C. J.; and Evenson, K. M.: Laser Magnetic Resonance Study of HO_2 Chemistry, Trans. AGU EOS, vol. 58, no. 6, 1977, p. 464.

67. Shimazaki, Tatsuo; and Ogawa, Toshihiro: A Theoretical Model of Minor Constituent Distributions in the Stratosphere Including Diurnal Variations. J. Geophys. Res., vol. 79, no. 24, 1974, pp. 3411–3423.

68. Shimazaki, T.; and Whitten, R. C.: A Comparison of One-Dimensional Theoretical Models of Stratospheric Minor Constituents. Revs. Geophys. and Space Phys., vol. 14, no. 1, 1976, pp. 1–12.

69. Urey, H. C.; Dawsey, L. H.; and Rice, F. O.: The Absorption Spectrum and Decomposition of Hydrogen Peroxide by Light. J. Am. Chem. Soc., vol. 51, 1929, pp. 1371–1383.

70. Molina, Luisa T.; Schinke, Stanley D.; and Molina, Mario J.: Ultraviolet Absorption Spectrum of Hydrogen Peroxide Vapor. Geophys. Res. Lett., vol. 4, no. 12, 1977, pp. 580–582.

71. Cox, R. A.; Derwent, R. G.; and Hutton, A. J. L.: Significance of Peroxynitric Acid in Atmospheric Chemistry of Nitrogen Oxides. Nature, vol. 270, no. 5634, 1977, pp. 328–329.

72. Jesson, J. P.; Glasgow, L. C.; Filkin, D. L.; and Miller, C.: The Stratospheric Abundance of Peroxynitric Acid. Geophys. Res. Lett., vol. 4, no. 11, 1977, pp. 513–516.

73. McQuigg, Robert D.; and Calvert, Jack G.: Photodecomposition of CH_2O, CD_2O, CHDO, and CH_2O-CD_2O Mixtures at Xenon Flash Lamp Intensities. J. Am. Chem. Soc., vol. 91, no. 7, 1969, pp. 1590–1599.

74. Evans, W. F. J.; Kerr, J. B.; Wardle, D. I.; McConnell, J. C.; Ridley, B. A.; and Schiff, H. I.: Intercomparison of NO, NO_2, and HNO_3 Measurements with Photochemical Theory. Atmosphere, vol. 14, no. 3, 1976, pp. 189–198.

75. Anderson, J. G.; Margitan, J. J.; and Stedman, D. H.: Atomic Chlorine and the Chlorine Monoxide Radical in the Stratosphere: Three in situ Observations. Science, vol. 198, no. 4316, 1977, pp. 501–503.

76. Warneck, Peter: Cosmic Radiation as a Source of Odd Nitrogen in the Stratosphere. J. Geophys. Res., vol. 77, no. 33, 1972, p. 6589.

77. Strobel, Darrell F.: Odd Nitrogen in the Mesosphere. J. Geophys. Res., vol. 76, no. 34, 1971, p. 8384.

78. Crutzen, P. J.: The Influence of Nitrogen Oxides on the Atmospheric Ozone Content. Quart. J. Roy. Meteorol. Soc., vol. 96, no. 408, 1970, pp. 320–325.

79. Johnston, Harold: Reduction of Stratospheric Ozone by Nitrogen Oxide Catalysts from Supersonic Transport Exhaust. Science, vol. 173, no. 3996, 1971, pp. 517–522.

80. Duewer, William H.; Wuebbles, Donald J.; and Chang, Julius S.: Effect of NO Photolysis on NO_y Mixing Ratios. Nature, vol. 265, no. 5593, 1977, pp. 523–525.

81. Johnston, Harold S.; and Nelson, Herbert: Comment on NO_X Catalytic Ozone Destruction: Sensitivity to Rate Coefficients by W. H. Duewer; D. J. Wuebbles, H. W. Ellsaesser, and J. S. Chang. J. Geophys. Res., vol. 82, no. 18, 1977, pp. 2593–2598.

82. Rowland, F. S., Spencer, J. E.; and Molina, Mario J.: Stratospheric Formation and Photolysis of Chlorine Nitrate. J. Phys. Chem., vol. 80, no. 24, 1976, pp. 2711–2713.

83. Rowland, F. S.; Spencer, John E.; and Molina, Mario J.: Estimated Relative Abundance of Chlorine Nitrate Among Stratospheric Chlorine Compounds. J. Phys. Chem., vol. 80, no. 24, 1976, pp. 2713–2715.

84. Stolarski, R. S.; and Cicerone, R. J.: Stratospheric Chlorine: A Possible Sink for Ozone. Canad. J. Chem., vol. 52, no. 8, 1974, pp. 1610–1615.

85. Wofsy, Steven C.; and McElroy, Michael B.: HO_X, NO_X, and $C\ell O_X$: Their Role in Atmospheric Photochemistry. Canad. J. Chem., vol. 52, no. 8, 1974, pp. 1582–1591.

86. Hunten, Donald M.: Estimates of Stratospheric Pollution by an Analytic Model. Proc. National Acad. Sci., vol. 72, no. 12, 1975, pp. 4711–4715.

87. McElroy, Michael B.; Elkins, James W.; Wofsy, Steven C.; and Yung, Yuk Ling: Sources and Sinks for Atmospheric N_2O. Revs. Geophys. and Space Phys., vol. 14, no. 2, 1976, pp. 143–150.

88. Johnston, Harold S.: Analysis of the Independent Variables in the Perturbation of Stratospheric Ozone by Nitrogen Fertilizers. J. Geophys. Res., vol. 82, no. 12, 1977, pp. 1767–1772.

89. Luther, F. M.; and Wuebbles, D. J.: Effect of Multiple Scattering on Ozone Reduction by NO_X and CFM's. IAGA/IAMAP Joint Assembly, Seattle, Washington, August 22–September 3, 1977.

90. Chang, Julius S.: Simulations, Perturbations, and Interpretations. Proceedings of the Third Conference on the Climatic Impact Assessment Program, Feb. 26–March 1, 1974, A. J. Broderick and T. M. Hard, eds., U.S. Department of Transportation report DOT-TSC-OST-74-15, Nov. 1974, pp. 330–341.

91. Harries, J. E.: The Distribution of Water Vapor in the Stratosphere. Revs. Geophys. and Space Phys., vol. 14, no. 4, 1976, pp. 565–575.

92. Gleason, C. C.; Rogers, D. W.; and Bahr, D. W.: Experimental Clean Combustor Program, Phase II Final Report. NASA CR-134971, July 1976.

93. Roberts, R.; Peduzzi, A.; and Vitti, G. E.: Experimental Clean Combustor Program, Phase II Final Report. NASA CR-134969, Nov. 1976.

94. Lohmann, R. A.; and Riecke, G. T.: Analytical Screening of Low Emissions, High Performance Duct Burners for Supersonic Cruise Aircraft Engines. NASA CR-135157, Mar. 1977.

95. Howlett, R. A.; Johnson, J.; Sabatella, J.; and Sewall, T.: Advanced Supersonic Propulsion Study, Phase III Final Report. NASA CR-135148, Dec. 1976.

1. Report No. NASA RP-1026	2. Government Accession No.	3. Recipient's Catalog No.
4. Title and Subtitle AN ASSESSMENT OF THE EFFECT OF SUPERSONIC AIRCRAFT OPERATIONS ON THE STRATOSPHERIC OZONE CONTENT		5. Report Date August 1978
		6. Performing Organization Code
7. Author(s) I. G. Poppoff, R. C. Whitten, R. P. Turco,* and L. A. Capone†		8. Performing Organization Report No. A-7399
		10. Work Unit No. 198-30-02
9. Performing Organization Name and Address Ames Research Center, NASA Moffett Field, Calif. 94035		11. Contract or Grant No.
		13. Type of Report and Period Covered Reference Publication
12. Sponsoring Agency Name and Address National Aeronautics and Space Administration Washington, D. C. 20546		14. Sponsoring Agency Code

15. Supplementary Notes

*Research Scientist, R and D Associates, Marina del Rey, California
†Research Associate, San Jose State University, San Jose, California

16. Abstract

An assessment of the potential effect on stratospheric ozone of an advanced supersonic transport operations is presented. This assessment, which was undertaken because of NASA's desire for an up-to-date evaluation to guide programs for the development of supersonic technology and improved aircraft engine designs, uses the most recent chemical reaction rate data.

From the results of the present assessment it would appear that realistic fleet sizes should not cause concern with regard to the depletion of the total ozone overburden. For example, the NO_x emission of one type designed to cruise at 20 km altitude will cause the ozone overburden to increase by 0.03% to 0.12%, depending upon which vertical transport is used. These ozone changes can be compared with the predictions of a 1.74% ozone decrease (for 100 Large SST's flying at 20 km) made in 1974 by the FAA's Climatic Impact Assessment Program.

17. Key Words (Suggested by Author(s)) Supersonic transport Stratosphere Ozone Photochemistry	18. Distribution Statement Unlimited STAR Category — 47	
19. Security Classif. (of this report) Unclassified	20. Security Classif. (of this page) Unclassified	21. No. of Pages 60	22. Price* $4.50